

1 **A Holocene temperature (brGDGT) record from Garba**
2 **Guracha, a high-altitude lake in Ethiopia.**

3 Lucas Bittner¹, Cindy De Jonge², Graciela Gil-Romera^{3,4}, Henry F. Lamb^{5,6}, James M. Russell⁷,
4 Michael Zech¹

5 ¹) Heisenberg Chair of Physical Geography with focus on paleoenvironmental research, Institute of Geography,
6 Technische Universität Dresden, Dresden, Germany

7 ²) Geological Institute, Department of Earth Sciences, ETH Swiss Federal Institute of Technology, 8092 Zurich,
8 Switzerland

9 ³) Plant Ecology and Geobotany dept., Philipps-Marburg University, Marburg, Germany.

10 ⁴) Department of Geo-environmental Processes and Global Change, Pyrenean Institute of Ecology, CSIC, Zaragoza,
11 Spain

12 ⁵) Department of Geography and Earth Sciences, Aberystwyth University, Aberystwyth, UK.

13 ⁶) Department of Botany, School of Natural Sciences, Trinity College Dublin, Dublin 2, Ireland

14 ⁷) Department of Geological Sciences, Brown University, USA

15 *Correspondence to:* Lucas Bittner (lucas.bittner@tu-dresden.de)

16

17

18

19

20

21

22

23

24 **Abstract.** Eastern Africa has experienced strong climatic changes since the last deglaciation (15,000 years ago). The
25 driving mechanisms and teleconnections of these spatially complex climate variations are yet not fully understood.
26 Although previous studies on lake systems have enhanced our knowledge of Holocene precipitation variation in eastern
27 Africa, relatively few studies have reconstructed the terrestrial temperature history of eastern Africa from lake archives.
28 Here, we present (i) a new branched glycerol dialkyl glycerol tetraether (brGDGT) temperature calibration that
29 includes Bale Mountain surface sediments and (ii) a quantitative record of mean annual temperature (MAT) over the
30 past 12 cal ka BP using brGDGTs in a sediment core collected from Garba Guracha (3950 m a.s.l.) in the Bale
31 Mountains. After adding Bale Mountain surface sediment (n=11) data to the existing East African lake dataset,
32 additional variation in 6-methyl brGDGTs was observed, which necessitated modifying the MBT'_{5ME} calibration by
33 adding 6-methyl brGDGT IIIa' (resulting in the MBT-Bale Mountain index, $r^2=0.93$, $p<0.05$). Comparing the MBT'_{5ME}
34 and the new MBT-Bale Mountain index, our high-altitude Garba Guracha temperature record shows that warming
35 occurred shortly after the Holocene onset when the temperature increased by more than 3.0 °C in less than 600 years.
36 The highest temperatures prevailed between 9 and 6 cal ka BP, followed by a temperature decrease until 1.4 cal ka BP.
37 The reconstructed temperature history is linked to supraregional climatic changes associated with insolation forcing
38 and the African Humid Period (AHP), as well as with local anomalies associated with catchment deglaciation and
39 hydrology.

40

41 Keywords: paleolimnology; MAT; brGDGT, calibration, palaeoclimatology, eastern Africa

42 1. INTRODUCTION

43 The severity of the current climate change and its global implications have been widely discussed following the latest
44 report from the Intergovernmental Panel for Climate Change (IPCC) (IPCC, 2021). Uncertainty in future climate
45 projection highlights the need for the scientific community to use palaeoclimate to estimate climate baseline conditions
46 prior to human impact on climate (Neukom et al., 2019). Although palaeoclimatology has become a central discipline
47 in understanding current climate variability (Thompson et al., 2002), important areas of the planet remain understudied.
48 A partial understanding of global climate complexity can lead to biased views of natural systems (Hughes et al., 2021).
49 This is the case for the African continent in general and northeastern Africa in particular. Current climatic conditions
50 in eastern Africa vary significantly due to its complex topography and the influence of the Intertropical Convergence

51 Zone (ITCZ), the Indian Monsoon and the El Niño-Southern Oscillation (ENSO). All of these affect temperature and
52 the distribution, amount and timing of rainfall in the region, resulting in a wide range of climatic conditions from the
53 warm, dry and semi-arid conditions of northern Kenya, south-eastern Ethiopia, Djibouti and Somalia to the cool, humid
54 conditions of the western highlands (Hove et al., 2011; Nicholson, 2017; Lyon and Vigaud, 2017).

55
56 There is clear evidence indicating that, since the last glacial period, northern and eastern Africa experienced severe
57 climatic changes (Tierney et al., 2008, 2011a, 2017, 2013; Loomis et al., 2015; Wagner et al., 2018). Three major
58 climate events are the post-glacial warming (~15 ka BP), hydrological variability during the African Humid Period
59 (AHP) (15 -5 ka BP) (deMenocal et al., 2000) that lead to the greening of the Saharan Desert (Blom et al., 2009), and
60 the drying period near the beginning of the Meghalayan (4.2 ka BP) (Bini et al., 2019). The intensity and the timing of
61 these climatic changes varied regionally over northern and eastern Africa (Castañeda et al., 2016). While the driving
62 mechanisms and the regional differences are complex and not fully understood, evidence supports the view that
63 climatic changes in northern and eastern Africa were connected across the northern hemisphere (Tierney et al., 2013;
64 Tierney and Russell, 2007; Otto-Bliesner et al., 2014). These complex teleconnections and their global impact support
65 the importance of understanding long-term climate drivers in eastern Africa. Such knowledge will lead to better
66 assessments of the impacts and potential mitigation of the current and future climate change scenarios in this world's
67 understudied yet critical region.

68 While several studies have reconstructed the precipitation history in northern and eastern Africa over the last 15 cal ka
69 BP (Bittner et al., 2021; Costa et al., 2014; Jaeschke et al., 2020; Junginger et al., 2014; Morrissey and Scholz, 2014;
70 Tierney et al., 2011a; Trauth et al., 2018; Wagner et al., 2018), only a few have reconstructed the regional temperature
71 history in northern and eastern Africa (Castañeda et al., 2016; Morrissey et al., 2018; Berke et al., 2012a; Loomis et
72 al., 2017, 2012, 2015; Tierney et al., 2008, 2016). Moreover, there is a lack of terrestrial temperature reconstructions,
73 especially in the high altitudes and the Horn of Africa. The Bale Mountain, situated in the East of the Rift Valley, are
74 a valuable study site with the potential to enhance the paleoclimatic knowledge in an understudied region.

75 For terrestrial archives, different methods have been developed and applied based on pollen, chironomids, and lipid
76 biomarkers (Cheddadi et al., 1998; Wu et al., 2007; Chevalier and Chase, 2015; Bonnefille et al., 1992; Eggermont et
77 al., 2010; Schouten et al., 2007). Over the last 15 years, an innovative approach for temperature reconstructions
78 emerged based on branched glycerol dialkyl glycerol tetraethers (brGDGTs), membrane-spanning bacterial lipids

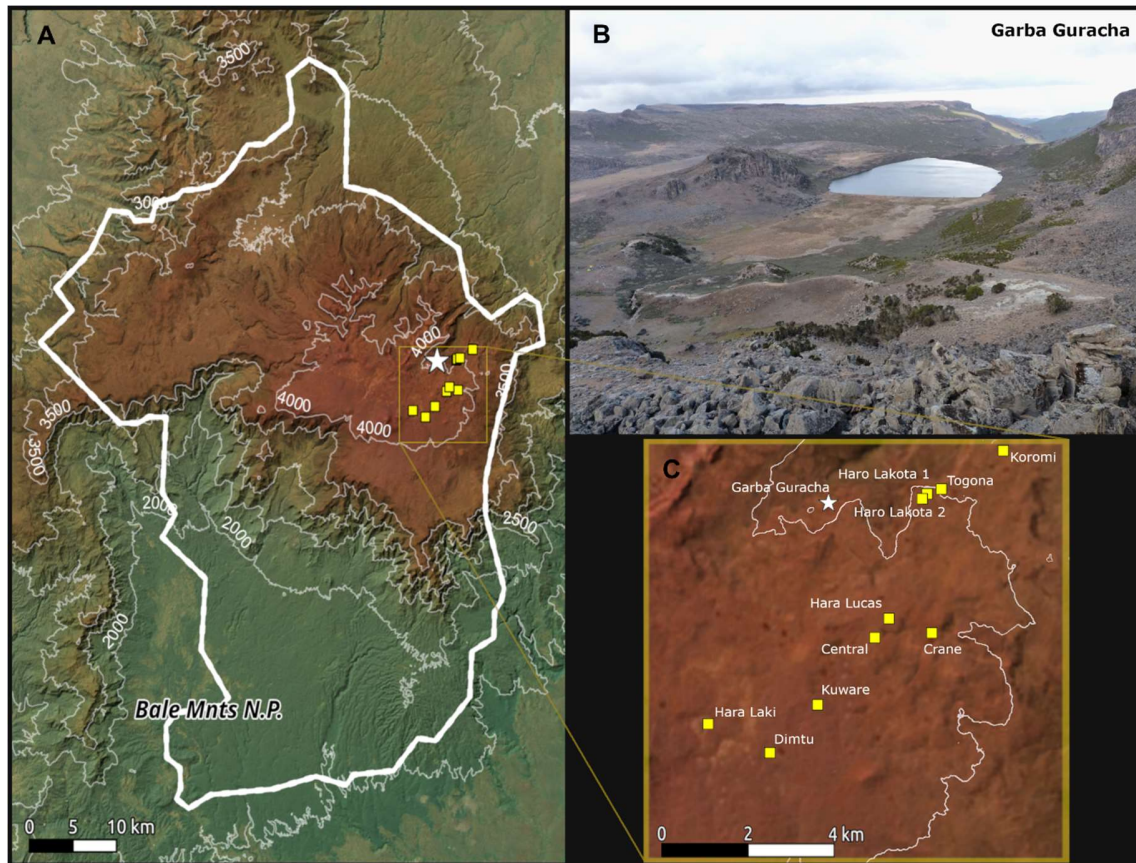
79 (Damsté et al., 2000). Several calibration studies in different settings (i.e. soils and lakes) have shown a correlation
80 between brGDGT abundances and mean annual air temperature (MAT) (e.g. De Jonge et al., 2014; Dearing Crampton-
81 Flood et al., 2020; Russell et al., 2018; Weijers et al., 2007). These calibrations have been successfully used to
82 quantitatively reconstruct continental temperature in marine river outflow and lacustrine sediments and terrestrial
83 archives such as loess sequences and paleosoils (Loomis et al., 2015, 2017; Schreuder et al., 2016; Zeng and Yang,
84 2019; Garelick et al., 2022). Recently, global calibrations have been developed that suit cooler and more seasonal high-
85 latitude lakes better (Martínez-Sosa et al., 2021; Raberg et al., 2021).

86 The phylogenetic breadth of the brGDGT-producing bacteria is still poorly constrained, although members from the
87 phylum Acidobacteria have been proposed to produce brGDGTs both in cultures and in the environment (Sinninghe
88 Damsté et al., 2018; De Jonge et al., 2019, 2021; Weber et al., 2018; van Bree et al., 2020). A recent study by Halamka
89 et al., 2021 reports that Acidobacteria produce certain brGDGTs under oxygen limitation. Originally, Weijers et al.
90 (2007b) found that the methylation (MBT) and cyclisation of branched tetraethers (CBT) correlate with the measured
91 mean annual air temperature (MAT) and pH values, respectively. Following the analytical separation of 5 and 6 methyl
92 isomers, De Jonge et al. (2014) developed a new modified MBT'_{5ME} ratio. This resulted in a revised calibration that
93 removed the pH dependence affecting the MBT/MAT correlation and improved the accuracy of MAT reconstructions
94 in terrestrial/soil archives. As brGDGT distributions recovered from lake sediments showed a different MAT
95 dependence compared to soils, Russell et al. (2018) developed a MBT'_{5ME} temperature calibration for lake sediments
96 in eastern Africa. However, compared to the dataset of Russell et al. (2018), the brGDGT distribution of some Bale
97 Mountain lake surface sediments are unique (Baxter et al., 2019). Although the MBT'_{5ME} calibration by Russell et al.
98 (2018) is a valuable supra-regional metric for reconstructing lake temperature, an adjusted calibration might better
99 account for local conditions in the Bale region.

100 In this study, we aim to (i) compare brGDGT distributions from lake surface sediments of the Bale Mountains (n=11)
101 (Baxter et al., 2019) with the eastern African dataset (Russell et al., 2018), (ii) develop a new ratio that captures the
102 unique variation in the Bale Mountains and compare the accuracy of this calibrated ratio with the MBT'_{5ME}, and (iii)
103 reconstruct the first Horn of Africa high altitude paleotemperature record in the Bale Mountains using the sedimentary
104 record of Garba Guracha (3950 m a.s.l.) and (iv) compare this Garba Guracha temperature record with other records
105 in the region.

106 **2. REGIONAL SETTINGS**

107 **2.1 Study area**



108
109 Figure 1: Location of the study area. (A) Bale Mountain National Park (thick white line), (B) a northeastward view over the glacial cirque of the
110 Garba Guracha catchment (Bittner et al., 2021), and (C) Bale Mountain lakes in the dataset (yellow) - The map was created by the authors using
111 QGIS 3.24 Tisler. All map layers are CC-by-SA v4.0, Image is from Bing Image / DigitalGlobe © Microsoft, DEM is from NASA/JPL SRTM
112 (<http://www.jpl.nasa.gov/srtm/>), and the Bale Mountains National Park boundaries are from © OpenStreetMap contributors 2019. Distributed under
113 the Open Data Commons Open Database License (ODbL) v1.0.

114
115 Garba Guracha (6.875781N, 39.878075E; Fig. 1) and all other lakes in this study are located east of the Main Ethiopian
116 Rift in the Bale Mountains of the Bale-Arsi Massif. More specifically, they are situated on the Sanetti Plateau, the
117 highest plateau in the Bale Mountains, between ~3800 to ~4200 m.a.s.l. and an area of 600 km² (Osmaston et al.,
118 2005). Solidified horizontal lava consisting of tuffs with rhyolites, alkali basalt, and trachyte formed the volcanic
119 plateau (Uhlig and Uhlig, 1991; Williams, 2016). The plateau and the valleys were partially glaciated at the Last
120 Glacial Maximum (Groos et al., 2021, 2020; Osmaston et al., 2005; Ossendorf et al., 2019). The glacial cirque Garba

121 Guracha was first mentioned by Werdecker (1962) and was also described in depth by Umer et al. (2007) and Tiercelin
122 et al. (2008). With a maximum water depth of 6 m and a very small catchment area, the lake is located at 3950 m above
123 sea level (0.15 km²; Fig. 1). The bedrock of the catchment is carbonate-poor (Löffler, 1978; Uhlig and Uhlig, 1991).
124 An outlet towards the Togona Valley is present during the rainy season at the lake's northern end. A swampy alluvial
125 plain fed by multiple springs stretches along the lake's southern shore.

126

127 **2.2 Climate**

128 The climate of the Bale Mountains varies spatially and temporally, affected by the orographic differences in altitude,
129 a north-south exposure and by changing atmospheric air mass movements over the course of the year (Kidane et al.,
130 2012; Uhlig and Uhlig, 1991). The Bale Mountains experience a four-month dry season (November to February) and
131 a long wet season with complex orographic rainfall patterns (March to October) (Woldu et al., 1989; Kidane et al.,
132 2012). The complexity of the rainfall pattern is associated with the convergence of northeast and southwest winds due
133 to the northern and southern location of the ITCZ between June and September and between October and March,
134 respectively (Tiercelin et al., 2008; Kidane et al., 2012). The Equatorial Westerlies and the Indian Ocean monsoon act
135 as two moisture sources for the precipitation in the Bale Mountains (Miehe and Miehe, 1994; Uhlig, 1988). With 1000-
136 1500 mm per year, the southern part of Bale Mountain experiences the highest precipitation amount, whereas the
137 northern region, including Garba Guracha, only receives 800-1000 mm (Woldu et al., 1989). Temperatures vary
138 seasonally, with the lowest temperatures in the dry season and the highest temperatures in the rainy season (Hillman,
139 1988). The Afro-Alpine regions, including the Sanetti Plateau, are characterised by diurnal temperature differences
140 between day and night (-15 to +26°C) (Hillman, 1988). Across the Bale Mountains, climate data has been collected
141 since 2017 with a mean annual temperature of 4.9 °C (max. 6°C; min. 3.4 °C) at the Angesso Station, located at the
142 same altitude 4 km northeast of Garba Guracha. The mean annual temperature at Garba Guracha is 5.4°C (Baxter et
143 al., 2019).

144

145 **3. MATERIAL AND METHODS**

146 **3.1. Material and Sampling**

147 In this study, we used the published data of 76 surface sediment samples from eastern African lakes. The data of these
148 lakes, located mainly in Ethiopia, Uganda and Kenya, were published by Loomis et al. (2014, 2011, 2012), Russell et
149 al. (2018), Eggermont et al. (2011) and Baxter et al. (2019). The environmental data for the 11 lakes in the Bale
150 Mountains were published by Eggermont et al. (2011) and Baxter et al. (2019), and the corresponding MAT is based
151 on a calculated lapse rate supported by local climate station data (Loomis et al., 2012; Russell et al., 2018).

152 At the Garba Guracha site, two overlapping sediment cores were retrieved in February 2017, at a water depth of 4.8 m
153 using a Livingstone piston corer. A maximum sediment depth of 1550 cm was reached, covering an organic matter-
154 rich upper section (0-900 cm) and an organic matter-poor bottom one (900-1550 cm). This study focuses on the last
155 12.3 cal ka BP covering the 0-950 cm, with a mean sedimentation rate of 15 years/cm (more details on sediment
156 properties and chronology can be found in Bittner et al. (2020)). We sampled at contiguous 10 cm intervals (average
157 ~100 years of sedimentation). Thirty-five samples were selected for brGDGT analyses.

158 **3.2 Sample preparation and analysis**

159 The total lipid extracts (TLE) of the surface sediment samples were extracted using an accelerated solvent extractor
160 (ASE) with dichloromethane:methanol in a ratio of 9:1 (Loomis et al., 2012). The brGDGTs were purified and
161 separated according to their polarity. The samples were quantified following the method described by Huguet et al.
162 (2006).

163 The TLE of the downcore sediments was obtained using a soxhlet system by constant rinsing (24h) with solvent
164 (dichloromethane:methanol in a ratio of 9:1). After rotary evaporation, the TLE was redissolved in *n*-hexane and
165 transferred onto a pipette column filled with aminopropyl silica gel (Supelco, 45 µm). Solvents of increasing polarity
166 (*n*-hexane, dichloromethane/methanol 2:1; diethyl ether/acetic acid 19:1) were used to selectively elute the fractions
167 of the TLE (nonpolar fraction A; two polar fractions B and C, including brGDGTs). Fraction B contained 98-99%,
168 while fraction C contained 1-2% of all brGDGTs. All results refer to the brGDGTs contained in fraction B. Before
169 measurement, a C₄₆ brGDGT standard was added, and the extract dried, redissolved in *n*-hexane/isopropanol (99:1)
170 and filtered using a 0.45 µm polytetrafluoroethylene (PTFE) filter. The measurements of the GDGTs (dissolved in *n*-
171 hexane/IPA (99:1)) were done at ETH Zurich using a high-performance liquid chromatograph (Agilent 1260) coupled

172 to a quadrupole mass spectrometer configured for atmospheric pressure chemical ionisation (HPLC-APCI-MS). The
 173 separation of the GDGTs was achieved by two silica columns at 45°C (modified after Hopmans et al. (2016)) with a
 174 flow rate of 0.2ml/min and an injection volume of 10 µl. Compound-peak integrations of m/z 1292, 1050, 1048, 1046,
 175 1046, 1034, 1032, 1022, 1020, 1018 and 744 were performed according to previously published methods (Hopmans
 176 et al., 2016).

177 3.3 BrGDGTs – structure, statistical methods and proxy calculation

178 BrGDGTs can be present as tetra- (I), penta- (II), or hexamethylated (III) compounds with different numbers of
 179 cyclopentyl moieties (none (a), one (b), or two (c)). The outer methyl group can be positioned on the α and/or ω C5
 180 (5-methyl compounds) or C6 (6-methyl compounds, indicated by a prime notation) location (De Jonge et al., 2014).
 181 To interpret the GDGT composition of the samples, we used the BIT, MBT', MBT'_{5ME}, and CBT' (Table 1).

182 We calculated the BIT index following the equation of Hopmans et al. (2004):

$$183 \text{ BIT index} = (Ia + IIa + IIIa + IIa' + IIIa') / (Ia + IIa + IIIa + IIa' + IIIa' + \text{crenarchaeol}) \quad [\text{Eq. 1}]$$

184 De Jonge et al. (2014) showed that the MBT' ratio (Peterse et al., 2012) contains 5- and 6-methyl compounds that are
 185 explicitly mentioned here:

$$186 \text{ MBT}' = (Ia + Ib + Ic) / (Ia + Ib + Ic + IIa + IIa' + IIb + IIb' + IIc + IIc' + IIIa + IIIa') \quad [\text{Eq. 2}]$$

187 By removing the 6 methyl isomers from the equation, De Jonge et al. (2014) improved the temperature calibration
 188 further:

$$189 \text{ MBT}'_{5ME} = (Ia + Ib + Ic) / (Ia + Ib + Ic + IIa + IIb + IIc + IIIa) \quad [\text{Eq. 3}]$$

190 The cyclisation of branched tetraethers (CBT') is calculated following the equation from De Jonge et al. (2014a):

$$191 \text{ CBT}' = {}^{10}\log((Ic + IIa' + IIb' + IIc' + IIIa' + IIIb' + IIIc') / (Ia + IIa + IIIa)) \quad [\text{Eq. 4}]$$

192 Russell et al. (2018) defined a calculation for surface water pH:

$$193 \text{ Surface water pH} = 8.95 + 2.65 * \text{CBT}' \quad [\text{Eq. 5}]$$

194 Lake water conductivity can be calculated using Eq. 12 of Raberg et al. (2021):

$$195 \ln(\text{conductivity}) = 6.62 + 8.87 * (Ib / (Ia + Ib + Ic))$$

$$196 \quad + 5.12 * ((IIa' / (IIa + IIb + IIc + IIa' + IIb' + IIc'))^2)$$

$$197 \quad + 10.64 * ((IIa / (IIa + IIb + IIc + IIa' + IIb' + IIc'))^2)$$

$$\begin{aligned}
198 \quad & - 8.59 * (IIa/(IIa + IIb + IIc + IIa' + IIb' + IIc')) \\
199 \quad & - 4.32 * ((IIIa'/(IIIa + IIIb + IIIc + IIIa' + IIIb' + IIIc'))^2) \\
200 \quad & - 5.31 * ((IIIa/(IIIa + IIIb + IIIc + IIIa' + IIIb' + IIIc'))^2) \\
201 \quad & - 142.67 * ((IIIb/(IIIa + IIIb + IIIc + IIIa' + IIIb' + IIIc'))^2) \quad [\text{Eq. 6}]
\end{aligned}$$

202

203 The fractional abundance of any individual brGDGT compound (i) was defined as:

$$204 \quad f(i) = i/(Ia + Ib + Ic + IIa + IIa' + IIb + IIb' + IIc + IIc' + IIIa + IIIa' + IIIb + IIIb' + IIIc + IIIc')[\text{Eq. 7}]$$

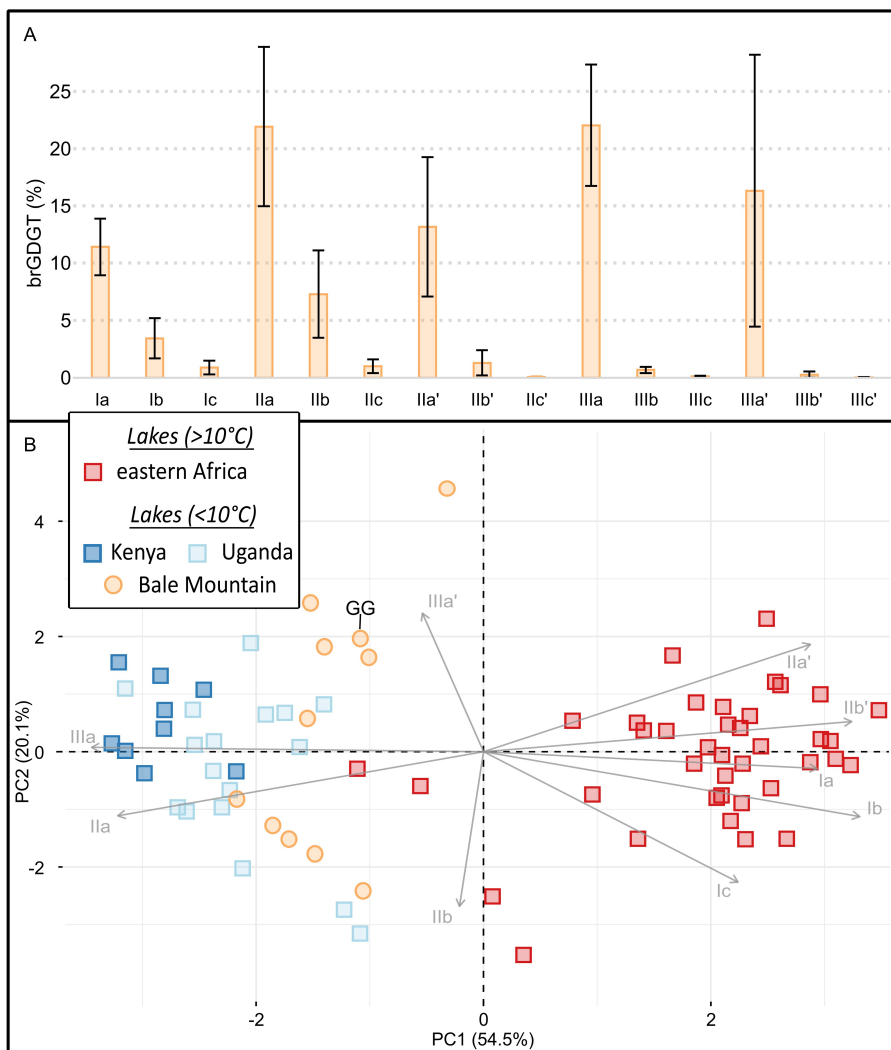
205

206 3.4 Quantitative data analyses

207 Numerical analyses in this paper have been performed with Excel and R 4.1.0 (R Core Team, 2021). Results are
208 displayed using the arithmetic mean and standard deviations using the notation \pm . To explore the correlations between
209 brGDGTs and MAT, we used linear regressions and the reported Pearson correlation values (r^2), where correlations
210 were considered significant when the p-value < 0.05 . We performed a Principal Component Analysis (PCA) of
211 brGDGTs from i) the calibration dataset and ii) the Garba Guracha record, based on standardised and scaled fractional
212 abundance. The ordination methods provide a simple yet effective way to visualise the variability within the
213 distribution of the brGDGTs. PCA was performed with the R package *factoextra* (Kassambara and Mundt, 2020).

214 **4. RESULTS**

215 **4.1 BrGDGT patterns of surface sediments from lakes in the Bale Mountains**



216
 217 Figure 2: (A) Barplot of average brGDGT percentages in Bale Mountain lake surface sediments (Baxter et al., 2019), with standard deviation, plotted
 218 as error flags, and (B) PCA of brGDGTs of eastern African lakes with regional pattern; data from Russell et al. (2018) and Baxter et al. (2019) -
 219 lakes >10°C (red) and lakes <10°C (Bale Mountain - orange, Kenya - blue and Uganda - light blue); Garba Guracha (GG).

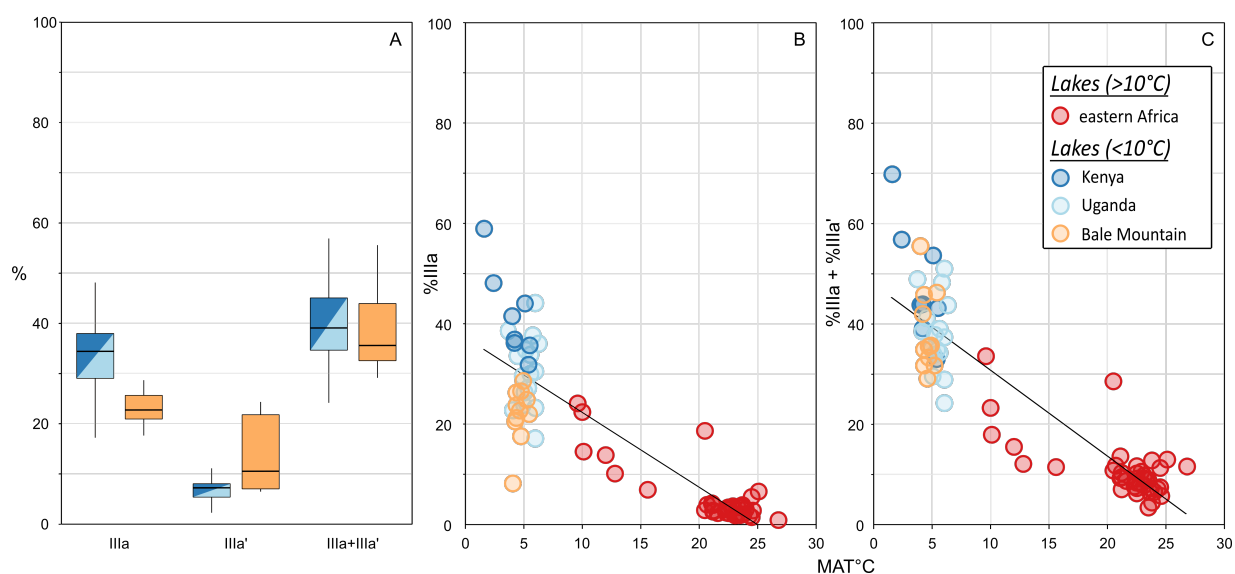
220
 221 To frame the downcore variation in Garba Guracha in the current environmental settings, we have expanded the dataset
 222 of Russell et al. (2018) by 11 Bale Mountain lake surface sediment samples (Table S1 and S2) (data from Baxter et
 223 al., 2019). Due to the missing values of IIc, IIc', IIIb, IIIb', IIIc and IIIc' in the manuscript by Russell et al. (2018), we

224 excluded these isomers in the Bale Mountain data from the PCA to allow direct comparison of the PCAs (see the
225 supplementary Figure S1 for different PCA including all isomers). The highest fractional abundances of brGDGTs in
226 these surface sediments are (i) IIIa with a mean of 22% (± 5), (ii) IIa with a mean of 22% (± 7) and (iii) IIIa' with a
227 mean of 16% (± 12) (Fig. 2A, Table S2).

228 The PCA of brGDGTs shows some differences between the East African lake dataset and the Bale Mountain lakes
229 (Fig. 2B). IIIa and IIa have negative loadings, and IIa', IIb', Ia, Ib and Ic have positive loading on PC1. PC2 shows
230 negative loadings from IIb and positive loading from IIIa' and IIa'. The Bale Mountain lakes have a negative score on
231 PC1, consistent with their location in a cool climate. The similar distribution of tetra-, penta- and hexamethylated
232 brGDGTs in surface sediments, illustrates a shared dominant lake-derived provenance as the East African lake dataset,
233 as soil-derived brGDGTs are characterised by a larger fractional abundance of brGDGTs Ia (Russell et al., 2018). At
234 the same time, the Bale Mountain lakes have a wide dispersion on PC2, illustrating additional variation of brGDGTs.
235 Regional differences in the brGDGT isomer abundances, especially in Bale Mountain surface sediments, are further
236 supported by variations in the degree of cyclisation (DC') and CBT' ratio values in the eastern African lake surface
237 sediment data (Russell et al., 2018; Baxter et al., 2019) (Fig. S2). Specifically, on PC2, a decrease IIb and an increase
238 of IIIa' is visible in some of the Bale Mountain lakes, including Garba Guracha (highlighted in Fig. 2B).

239 Compared to similar high-altitude lakes (above 3500 m and MAT < 10°C) in eastern Africa (Kenya and Uganda lakes
240 previously published in the East African lake dataset (Russell et al., 2018)), the percentage of IIIa and IIa is lower, and
241 the percentage of IIIa' and IIa' is higher in the Bale Mountain lakes (Fig 3). Interestingly, the combined percentage of
242 these 5 and 6 methyl isomers is similar (Fig. 3A).

243



244
 245 Figure 3: (A) Abundance (%) of IIIa and IIIa'; (B) Linear correlation between IIIa (%) and MAT ($r^2 = 0.78$) and (C) IIIa + IIIa' (%) to MAT ($r^2 =$
 246 0.82) - data from Russell et al. (2018) and Baxter et al. (2019) - lakes $>10^\circ\text{C}$ (red) and lakes $<10^\circ\text{C}$ (Bale Mountain - orange, Kenya - blue and
 247 Uganda - light blue).

248
 249 We hypothesise that the 6-methyl compound (IIa' and IIIa') might be produced instead of their 5-methyl counterparts
 250 (IIa and IIIa), resulting in their higher fractional abundance in some of the Bale Mountain lakes (Fig. 3A). This is
 251 supported by our observation that, in the East African lake dataset, the correlation of %IIIa to MAT ($r^2 = 0.78$) is
 252 slightly improved by adding %IIIa' to $r^2 = 0.82$ (Fig 3 B, C). Narrowing the temperature range, ($\text{MAT} < 10^\circ\text{C}$), the
 253 improvement remains significant: the correlation of %IIIa to MAT ($r^2 = 0.11$; $p\text{-value} < 0.001$) is improved by adding
 254 %IIIa' to $r^2 = 0.31$ ($p\text{-value} < 0.001$) (Fig. S3). Although the production of IIIa' at the expense of IIIa is poorly
 255 understood in lacustrine settings the isomerisation of brGDGTs can be affected by the conductivity and salinity of the
 256 lake water (Raberg et al., 2021; Wang et al., 2021). As IIIa is a major component of the $\text{MBT}'_{5\text{ME}}$ ratio, the hypothesised
 257 production of IIIa' at the expense of IIIa could have the potential to influence $\text{MBT}'_{5\text{ME}}$ values. Indeed, $\text{MBT}'_{5\text{ME}}$ values
 258 of the Bale Mountain lakes range from 0.20 to 0.37, with a mean of $0.24 (\pm 0.05)$. As the MAT range of Bale Mountain
 259 lakes is limited ($4\text{-}5.4^\circ\text{C}$), the range of $\text{MBT}'_{5\text{ME}}$ is larger than expected of the measured MAT relative to similar
 260 eastern African lakes in the East African lake dataset ($\text{MBT}'_{5\text{ME}} = 0.17$ to 0.25 with a mean of 0.22 ± 0.02 ; $\text{MAT} = 4\text{-}$
 261 5.4°C) (Russell et al., 2018).

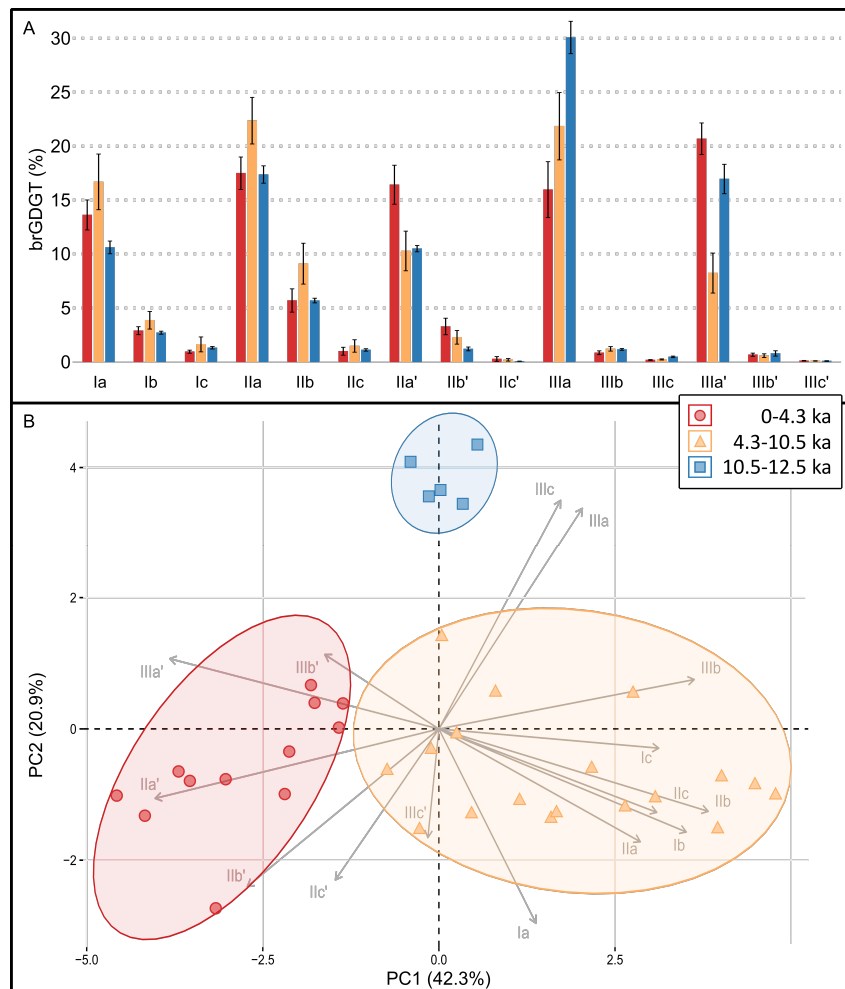
262 4.2 BrGDGT patterns of the Garba Guracha sediment core

263 In general, the sediments of the Garba Guracha are characterised by a high input of aquatic organic matter. Several
264 analysed proxies used to identify the source of organic matter indicate a predominantly aquatic production ($\delta^{13}\text{C}$,
265 TOC/N, P_{aq} , sugar quantification ratios) (Bittner et al., 2020, 2021). The composition of brGDGTs in the sediment of
266 Lake Garba Guracha is inconsistent with the soil samples in Bale Mountain, indicating different producing
267 communities (Fig. S4, Table S3). These findings are concurrent with the results of Russell et al. (2018) that brGDGTs
268 in eastern African lake sediments are dominantly lake-derived. Therefore, we suggest that most brGDGTs in the Garba
269 Guracha sediment archive are also of aquatic origin.

270 In the Garba Guracha sediments, both branched and isoprenoid GDGTs are present. The BIT index ranges between
271 0.8 and 1 (mean=0.98, ± 0.04). Only the oldest samples (12-10 cal ka BP) have a lower BIT index value of 0.8 to 0.9
272 (Table S4). Tetramethylated brGDGTs in the sediment core represent on average 19.5%, pentamethylated brGDGTs
273 44%, and hexamethylated brGDGTs 36.5% (Table S4). The highest fractional abundances are (i) IIIa with a mean of
274 21% (± 5), (ii) IIa with a mean of 20% (± 3) and (iii) Ia with a mean of 15% (± 3). The $\text{MBT}'_{5\text{ME}}$ ranges from 0.20 to
275 0.35 with a mean of 0.28 (± 0.04) (Table S5). The CBT' ratio ranges from 0.06 to -0.54 with a mean of 0.27 (± 0.18)
276 (Table S4).

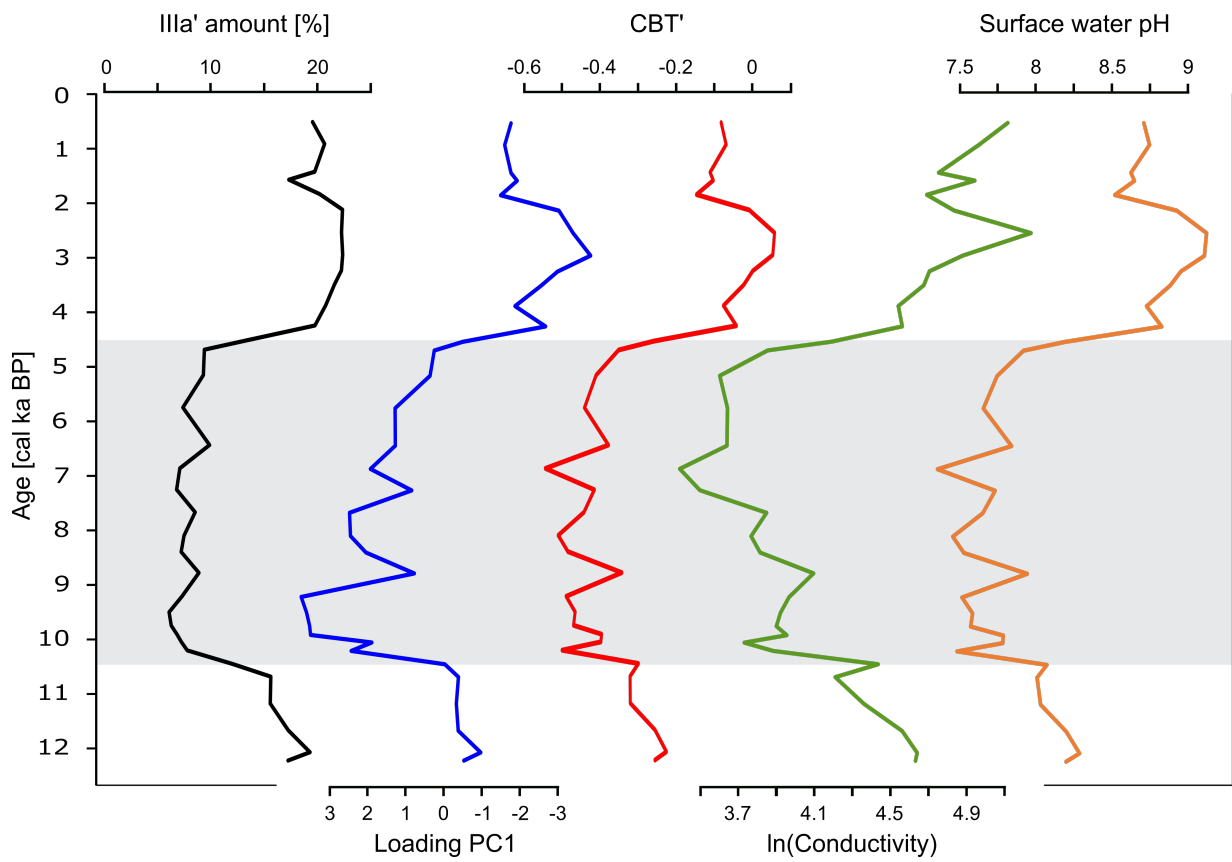
277 A PCA of all downcore brGDGTs distributions (Fig. 4A) shows that the first two components explain 63.2% of the
278 variance. On PC1 (42.3%), all 6 methyl isomers have negative loadings, while 5 methyl isomers show positive
279 loadings. PC2 (20.9%) shows positive loadings of all hexamethylated brGDGTs and negative loadings of all penta-
280 and tetramethylated brGDGTs. The PCA reveals changes in brGDGT composition with core depth when the data
281 points are grouped using the following age cut-offs: (0-4.3 cal ka BP; 4.3-10.5 cal ka BP; 10.5-12.5 cal ka BP) (Fig.
282 4A). In phase 1 (12.5 – 10.5 cal ka BP), IIIa, IIIa' and IIa have the highest mean abundances of 30%, 17%, and 17%,
283 respectively. In phase 2 (10.5 – 4.3 cal ka BP), the mean abundance of IIIa and IIIa' are decreased by around 9%, while
284 IIa, IIb and Ia increase. In phase 3 (4.3 – 0 cal ka BP), the mean abundances of IIIa decrease by 6% further. Conversely,
285 the mean abundance of IIIa' increases again by 12%. The same holds true for IIa (-5%) and IIa' (+6%). The mean
286 abundance of Ia increases further by 3% (Fig 4B).

287



288
 289 Figure 4: (A) barplot of average brGDGT percentages in the Garba Guracha sediment core, with standard deviation, plotted as error flags; (B) PCA
 290 of brGDGTs of the Garba Guracha sediment core; data from 0 to 4.3 cal ka BP (red), data from 4.3 to 10.5 cal ka BP (orange) and data from 10.5
 291 to 12.5 cal ka BP (blue).

292
 293 The unusually high abundance of brGDGTs IIIa' compared to IIIa observed in surface sediments of Bale Mountains
 294 lakes (Fig. 2A) is also visible in the Garba Guracha record and the relative abundance of IIIa' varies with depth. High
 295 amounts of IIIa' appear until 10.8 cal ka BP followed by low percentage (<10%) until 4.5 cal ka BP. The highest
 296 abundance of IIIa' with up to 22% occurs after 4.5 cal ka BP until the recent past. The changing abundances of IIIa' in
 297 our record coincide with changes in CBT' (Fig. 5). The variability in the 6-methyl brGDGTs reflects the largest part
 298 of the variation in this dataset, reflected by the good agreement ($r^2= 0.77$, $p<0.001$) between the fractional abundance
 299 of brGDGTs IIIa' and the sample loadings on PC1.



300
 301
 302 Figure 5: Downcore functions for Illa' amount, the PC1 loading, CBT', ln(conductivity) (Eq. 12 in Raberg et al., 2021), and surface water pH of the
 303 Garba Guracha brGDGT record.
 304

305 **5. DISCUSSION**

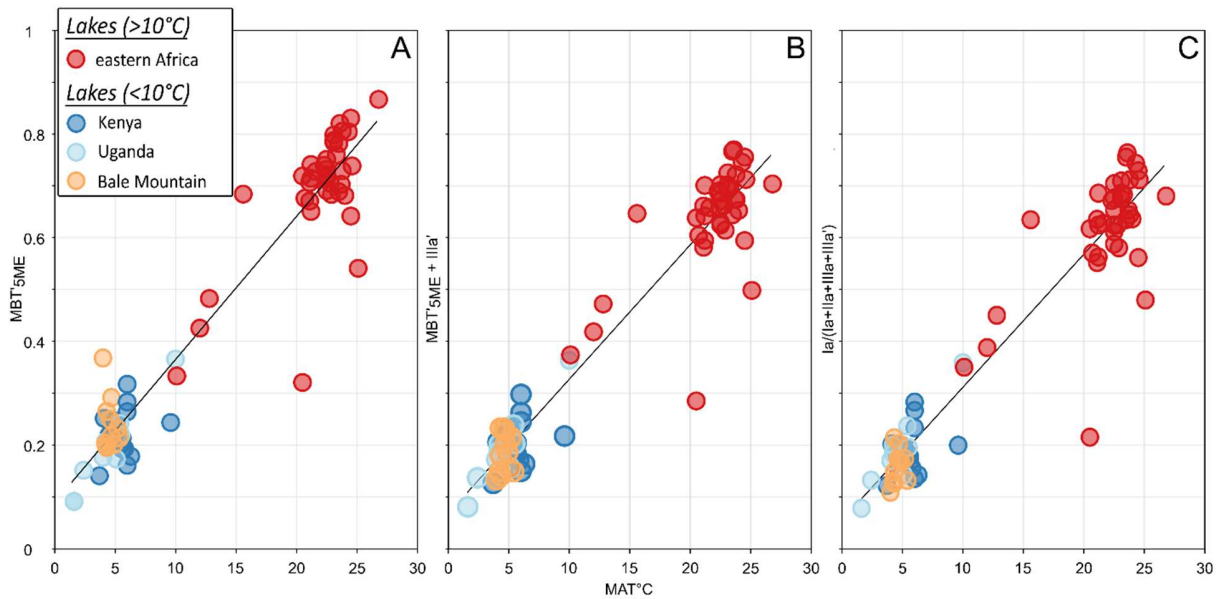
306 **5.1 Possible MAT calibration functions inferred from the expanded eastern African surface sediment dataset**

307 *Table 1: Temperature calibrations – Ratios, calibration dataset, r^2 , and root-mean-square-error (RMSE) in $^{\circ}\text{C}$ - East African Lake*
 308 *dataset (EAL), East African Lakes + Bale Mountain lakes (EAL_{BM})*

Ratio		Calibration dataset	r^2	RMSE $^{\circ}\text{C}$
MBT' _{5ME} (Ia+Ib+Ic)/(Ia+Ib+Ic+IIa+IIb+IIc+IIIa)		EAL (n=65)	0.92	2.41
		EAL _{BM} (n=76)	0.92	2.41
MBT' _{5ME} + IIIa' (Ia+Ib+Ic)/(Ia+Ib+Ic+IIa+IIb+IIc+IIIa+IIIa')	[Eq. 8]	EAL _{BM} (n=76)	0.93	2.38
Simplified MBT' _{5ME} + IIa'&IIIa' Ia/(Ia+IIa+IIIa+IIa'+IIIa')	[Eq. 9]	EAL _{BM} (n=76)	0.84	3.48
Simplified MBT' _{5ME} + IIIa' Ia/(Ia+IIa+IIIa+IIIa')	[Eq. 10]	EAL _{BM} (n=76)	0.91	2.59

309
 310 We added the GDGT distribution data of 11 surface sediments from Bale Mountain lakes (Baxter et al., 2019) to the
 311 existing data of Russell et al. (2018) and applied the MBT'_{5ME} calibration (Table 1). Here, the original dataset (n = 65)
 312 is referred to as East African Lakes "EAL", while the extended dataset (n = 76) is referred to as East African Lakes +
 313 Bale Mountain lakes (EAL_{BM}). The linear correlation between the MBT'_{5ME} and MAT was almost identical after adding
 314 the 11 Bale Mountain lake samples (EAL $r^2 = 0.92$, EAL_{BM} $r^2 = 0.92$). In the tropical Bale Mountain, the freezing of
 315 lakes is extremely rare, due in part to the intense year-round insolation, and MAT is equal to MAF. To test whether
 316 the unique brGDGT distribution in some Bale Mountain lakes (Fig. 2) affected the temperature correlation, we applied
 317 various calibrations to account for the increased abundance of IIIa' (and to a lesser extent IIa'). In the EAL_{BM} dataset,
 318 the application of this ratio has a lower r^2 of 0.84 and a higher RMSE of 3.48 $^{\circ}\text{C}$ compared to the MBT'_{5ME} (Table 1:
 319 Eq. 9). As brGDGT IIIa' specifically was shown to increase in Bale Mountain sediments and improved the correlation
 320 with MAT (Fig. 3B and C), we investigated alternative ratios that incorporate this compound but exclude IIa'. Table 1
 321 and Fig. 6 summarise the correlation coefficients of the MBT'_{5ME} ($r^2 = 0.92$, RMSE of 2.41 $^{\circ}\text{C}$), an MBT'_{5ME} ratio that
 322 includes IIIa' (Eq. 10) with $r^2 = 0.93$ and RMSE of 2.38 $^{\circ}\text{C}$ and the simplified ratio that includes only the major
 323 brGDGTs compounds (Eq. 10: $r^2 = 0.91$ and an RMSE of 2.59 $^{\circ}\text{C}$).

324

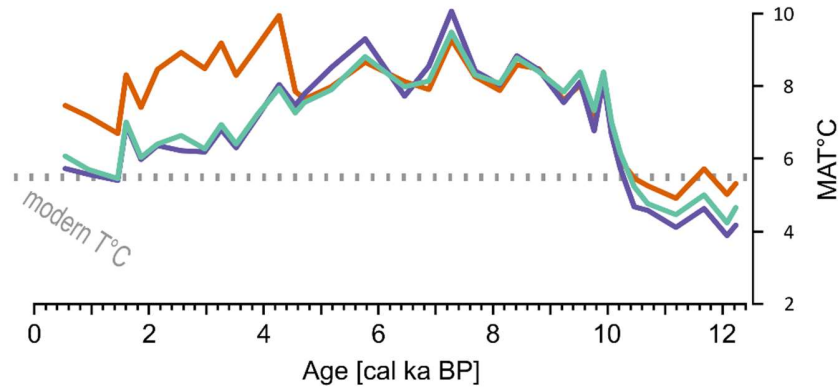


325
 326 Figure 6: Correlations EAL_{BM} datasets, (A) MBT'_{5ME} ($r^2 = 0.92$; RMSE of 2.41); (B) MBT'_{5ME} + IIIa' ($r^2 = 0.93$; RMSE of 2.38.); (C)
 327 Ia/(Ia+IIa+IIIa+IIIa') ($r^2 = 0.91$; RMSE of 2.59) - data from Russell et al. (2018) and Baxter et al. (2019) - lakes >10°C (red) and lakes <10°C (Bale
 328 Mountain - yellow, Kenya - blue and Uganda - light blue)

329 The results of the calibrations $Ia/(Ia+IIa+IIIa+IIIa')$ ($MAT = -0.773 + 35.646 \times Ia/(Ia+IIa+IIIa+IIIa')$) and $MBT'_{5ME} +$
 330 $IIIa'$ ($MAT = -1.4734 + 35.777 \times MBT'_{5ME} + IIIa'$) applied to the Garba Guracha sediment core are very similar and
 331 correlate well ($r^2=0.97$) (Fig. 7, purple and green curves, respectively). Therefore, we will only discuss the best
 332 performing calibrations developed using the EAL_{BM} dataset MBT'_{5ME} ($MAT = -1.8299 + 33.304 \times MBT'_{5ME}$) and the
 333 MBT'_{5ME} + IIIa' calibration to the downcore distributions.

334

335 **5.2 Paleotemperature reconstructions for the Garba Guracha sedimentary record - comparison of the different**
 336 **calibrations**



337
 338 Figure 7: Reconstructed temperatures of the Garba Guracha sedimentary record. MBT'_{5ME} (orange); Ia/(Ia+IIa+IIIa+IIIa') (purple); MBT'_{5ME} + IIIa'
 339 (turquoise).

340
 341 We evaluate the downcore trend in GG sediments to compare the performance of both calibrations, revealing periods
 342 of agreement (10-4.2 ka BP) and a period of temperature offset (since 4.2 ka BP). Using established and newly
 343 developed ratios and calibrations (MBT'_{5ME} + IIIa' and MBT'_{5ME} EAL_{BM}) resulted in similar absolute values and
 344 comparable temperature trends, principally in the early and mid-Holocene. Reconstructed temperatures range from 4.9
 345 to 10.0°C (MBT'_{5ME}) and 4.2 to 9.5°C (MBT'_{5ME} + IIIa') (Fig. 7). Despite a slightly different range in temperature (4.4
 346 and 5.3 °C), the trends of both calibrations are similar between 12 and 4.7 cal ka BP. The lowest MATs (< 5°C)
 347 occurred between 12.2 cal ka BP (950 cm) and 10.5 cal ka BP (800 cm). MAT increased rapidly by 3.5°C between
 348 10.5 cal ka BP (800 cm) and ca. 10 cal ka BP (700 cm). During the early to mid-Holocene, a thermal maximum
 349 occurred between 10 and 5.7 cal ka BP (440 cm), with the highest MAT values reaching ca. 10°C. At ~6.5 cal ka BP,
 350 the MAT decreased for both calibrations. The temperature drop coincides with organic-poor layers in the sediment
 351 core formed during a drought, associated with low monsoonal intensity (Bittner et al., 2020). A strong offset between
 352 the calibrations appeared at 4.2 cal ka BP, at a moment when temperatures are expected to decrease in phase with
 353 insolation (Fig. 7). Using the MBT'_{5ME}, we reconstruct a sudden temperature rise (Fig. 7) that contrasts with the
 354 temperature decrease when using the MBT'_{5ME} + IIIa' calibration. The offset coincides with a known drought phase and
 355 is accompanied by shifts of many proxies (TOC, δ¹³C, TOC/N, *Erica spp*, charcoal) in the Garba Guracha sediments
 356 (Bittner et al., 2020; Gil-Romera et al., 2019). The changing conditions in the Garba Guracha catchment during this

357 drought phase, especially the decline of the *Erica* shrubland (Gil-Romera et al., 2019), might have increased the surface
358 water pH (Fig.5). A change in the lake water chemistry is supported changes in the reconstructed surface water pH
359 (7.3-9.1) and conductivity (30 – 189; reported in Fig. 5 as ln(conductivity)) of the lake water (Fig. 5; calibrations from
360 Russel et al., 2018 and Raberg et al., 2021). In the last years, studies have suggested that the change in brGDGT
361 composition captured by the CBT' may change due to shifting bacterial communities in soils and lakes (De Jonge et
362 al., 2019; van Bree et al., 2020; Weber et al., 2018). Previously, pH, conductivity and salinity-dependent brGDGTs
363 composition, sometimes driven by community changes, have been shown to affect MBT'_{5ME} values in soils and lake
364 sediments (De Jonge et al., 2021; Wang et al., 2021; Raberg et al., 2021), and we propose that a similar effect can be
365 seen in Garba Guracha.

366 Hence we suggest that MBT'_{5ME} systematically overestimates the temperatures of Garba Guracha during the late
367 Holocene after 4 cal ka BP. A systematic offset is further supported by continuously and similarly decreasing
368 reconstructed temperatures using both calibrations until the top of the core with a shared maximum at 150 cm (1.6 cal
369 ka BP). We suggest that the production of IIIa' at the expense of IIIa is increased during dryer intervals, possibly caused
370 by a change in lake water chemistry and/or bacterial communities. We conclude that a temperature calibration
371 including IIIa' allows to reconstruct MAT in Garba Guracha sediments more accurately, as it accounts for the unique
372 and variable production of IIIa' in Bale Mountain lakes.

373 **5.3 Paleotemperature reconstructions for the Garba Guracha sedimentary record – regional comparison**

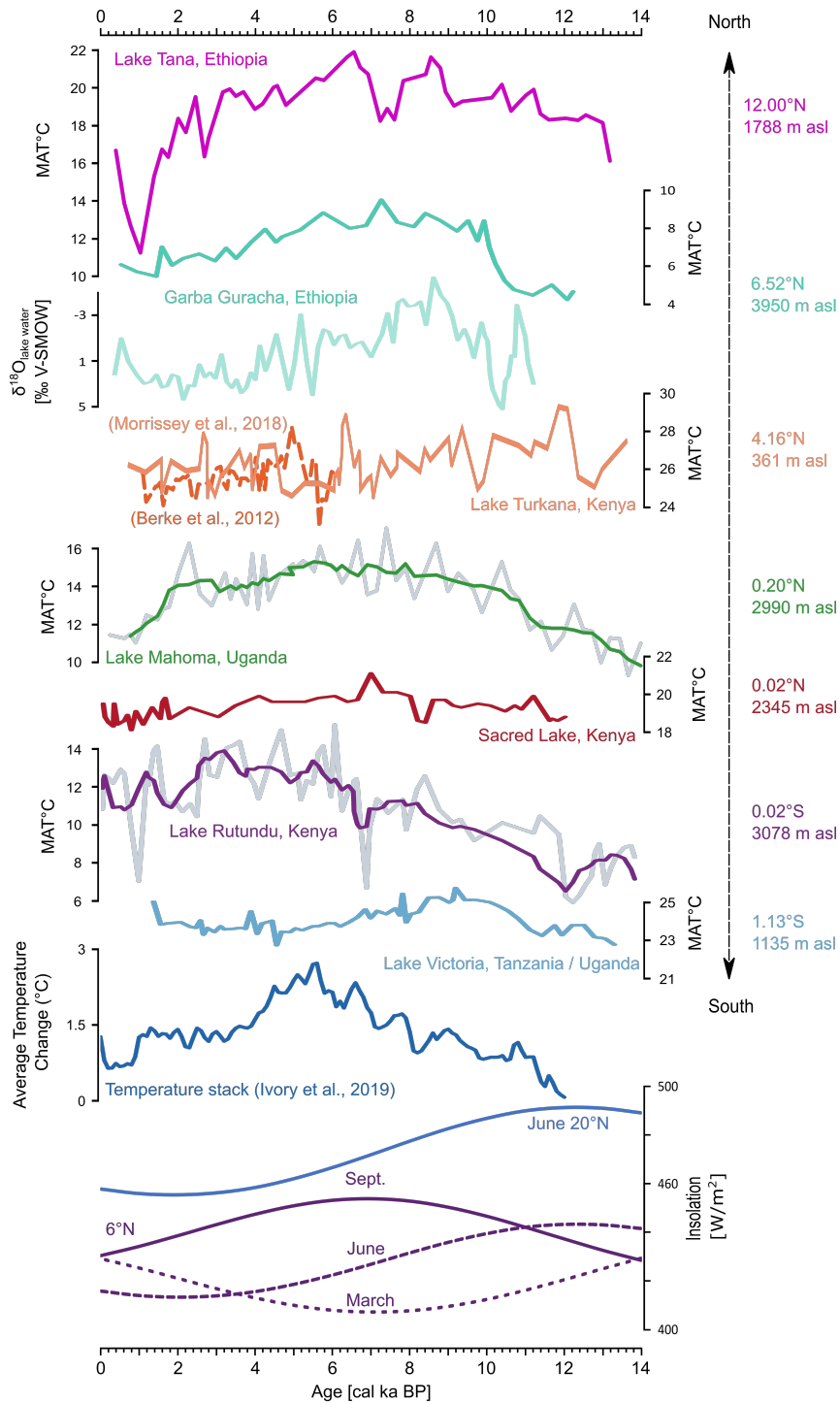
374 In contrast to precipitation reconstructions based on $\delta^2\text{H}$ in East Africa (Garelick et al. 2021), the temperature records
375 do not show a clear meridional, north-south temperature change, nor an east-west pattern. The reconstructed overall
376 temperature ranges are, however, consistent with the elevations of the lake archives. The amplitude of temperature
377 change over the last 13 ka at Garba Guracha is $\sim 6^\circ\text{C}$. Similar amplitudes of change have been reconstructed at other
378 high-altitude sites (Lake Mahoma and Lake Rutundu) (Loomis et al. 2017; Garelick et al. 2022), whereas equatorial
379 records at lower elevations yield lower temperature amplitudes (Lake Victoria and Lake Tanganyika) (Tierney et al.
380 2008; Berke et al. 2012), and higher temperature amplitudes are also recorded in northeast African Lake Tana (Loomis
381 et al. 2015). In fact, Garba Guracha has some of the highest amplitude temperature changes of all of the sites during
382 the Holocene, perhaps because it combines high elevation with a slightly higher latitude than other terrestrial African
383 temperature records.

384 5.3.1. Deglacial warming

385 Overall, the recorded temperature trends in Garba Guracha are in phase with northern summer insolation variability
386 (Fig. 8). This is reasonable because air temperature and insolation are closely connected (Huybers, 2006). However,
387 the coldest MATs ($<5^{\circ}\text{C}$) were recorded before 10.5 cal ka BP even though the northern hemisphere summer (20°N)
388 insolation maxima occurred already 12 cal ka BP (Fig. 8). Tiercelin et al. (2008) argue that in Garba Guracha, ice
389 remained in the catchment until ~ 10 cal ka BP due to topographical conditions, especially the north-facing exposition
390 of the valley. The remaining ice in the basin might have (i) reduced the temperature of the lake water by inflow of cold
391 melt water and (ii) buffered the air temperature warming caused by increasing insolation. Indeed, rising temperatures
392 were recorded in other eastern African records as early as 21 cal ka BP (Lake Mahoma) (Garelick et al., 2022) and in
393 Ethiopia as early as 14 cal ka BP (Lake Tana) (Loomis et al., 2015; Tierney et al., 2016).

394 Similar to Lake Tana, but ~ 4000 years later, MAT ($^{\circ}\text{C}$) in the Garba Guracha record experienced an abrupt increase
395 of ca. 3.5°C in just ca. 600 years, from 10.5 to 9.9 cal ka BP. Simultaneously with the rise in temperature, Bittner et
396 al. (2021) found an increase in P/E, indicating higher moisture availability based on depleting values of reconstructed
397 $\delta^{18}\text{O}_{\text{lake water}}$. At Lake Tana, Loomis et al. (2015) and Costa et al. (2014) attribute a similar connection between warmer
398 temperature and depleted water isotopes ($\delta^2\text{H}$) since 13.8 cal ka BP to the penetration of warm Congo Basin air masses
399 resulting in weaker easterly trade winds and a strengthening of the southwesterly winds and the Somali Jet. The con-
400 nection between Congo Basin air masses and eastern Africa is supported by the absence of cold temperatures associated
401 with the Younger Dryas (YD) in both the Congo Basin temperature record (Weijers et al., 2007a) and Lake Tana
402 (Loomis et al., 2015). However, in the Garba Guracha record, lower temperatures prevailed 4000 years longer than in
403 Lake Tana (Loomis et al., 2015). Although catchment glaciers could have caused these conditions in Garba Guracha,
404 the low temperatures are accompanied by a reduced sedimentation rate between 12.8 and 11.3 cal ka BP (Bittner et al.,
405 2020), pointing to climatic influences associated with YD times (Alley, 2000). Indeed, other records from the Horn of
406 Africa indicate dry conditions associated with the YD period, like Lake Ashenge (Marshall et al., 2009) and the marine
407 record of the Gulf of Aden (Tierney and deMenocal, 2013). Therefore, we suggest that, at least for some periods, the
408 climate drivers operating in the Garba Guracha region might have been different from other parts of eastern Africa.
409 The time lag between Lake Tana and Garba Guracha could be explained by a slow eastwards advance of the Congo
410 Air Boundary and different climatic conditions at the sites. However, with the current data, we are unable to precisely

411 distinguish between north hemisphere YD forcing, remaining ice in the lake catchment, or regional atmospheric cir-
 412 culation change affecting the Garba Guracha record.



413

414 Figure 8: Comparison of records. MAT: Lake Tana (Loomis et al., 2015); Garba Guracha (this study); $\delta^{18}\text{O}_{\text{lake water}}$ as reconstructed from the aquatic
415 sugar biomarker fucose (Bittner et al., 2021); Lake Turkana (Berke et al., 2012; Morrissey et al., 2018); Lake Mahoma (Garelick et al., 2022); Sacred
416 Lake (Loomis et al., 2012); Lake Rutundu (Loomis et al., 2017); Lake Victoria (Berke et al., 2012); eastern Africa temperature stack (Ivory et al.,
417 2019); and insolation 6°N and June 20°N (Laskar et al., 2004).

418 5.3.2. Warm temperatures during the African Humid Period in eastern Africa

419 Regardless of the cause, the ~10.5 cal ka BP rise in MAT is associated with an abrupt increasing moisture availability
420 and changes of vegetation around Garba Guracha (Gil-Romera et al., 2021; Umer et al., 2007). Vegetation and fire
421 dynamics around Garba Guracha responded dynamically to the changing climatic conditions, evidencing the sensitivity
422 of the afroalpine-afroalpine plant communities to increasing temperature. As MAT increased between 11 and 10 cal
423 ka BP, the ericaceous belt expanded (Gil-Romera et al., 2021). The rising temperature and increasing P/E (Bittner et
424 al., 2021) were accompanied by the expansion of the afroalpine vegetation cover (Gil-Romera et al., 2021; Miehe and
425 Miehe, 1994). An immediate consequence of the temperature rise and increasing moisture availability was biomass
426 accumulation, as evidenced by the change from organic matter-poor to organic matter-rich sedimentation (Bittner et
427 al., 2020) and the expansion of heathlands (Gil-Romera et al., 2019). Under an increasing MAT and extending biomass,
428 fire activity was very intense at this time (Gil-Romera et al., 2019).

429 The thermal maximum of the Garba Guracha record spanned from 9 to 5.8 cal ka BP, with the highest reconstructed
430 temperatures occurring at 7 cal ka BP. A similar mid-Holocene thermal optimum has been recorded at Sacred Lake (7
431 cal ka BP) and Lake Tana (7 cal ka BP) (Fig 8). However, the highest temperatures of Lake Victoria occurred at 9 cal
432 ka BP, and of Lake Rutundu, Lake Malawi and Lake Tanganyika at 5 cal ka BP (Berke et al., 2012b; Loomis et al.,
433 2017, 2015, 2012; Powers et al., 2005; Tierney et al., 2008; Garelick et al., 2022). At Lake Turkana, the thermal
434 optimum occurred at 6.4 cal ka BP (Morrissey et al., 2018) or 5 cal ka BP (Berke et al., 2012a). A new temperature
435 reconstruction from Lake Mahoma (Garelick et al., 2022) and a temperature stack including temperature reconstruc-
436 tions from Sacred Lake, Lake Malawi, Lake Tanganyika, Lake Rutundu, and the Congo Basin by Ivory and Russell
437 (2018) showed the highest temperatures between ~7 and ~4.5 cal ka BP. The timing of the highest reconstructed tem-
438 peratures at these sites is not related to greenhouse gas radiative forcing or insolation forcing (Loomis et al., 2015).
439 Loomis et al. (2015) point out that the Lake Tana and Sacred Lake temperature maxima lag northern hemisphere
440 summer insolation, and Lake Malawi and Lake Tanganyika lead peak southern summer insolation. In the case of Garba
441 Guracha, the highest temperatures coincide with local maximum September insolation at the sites latitude of 6°N

442 (Laskar et al., 2004) (Fig. 8). This matches the suggestion of Berke et al. (2012a) that the thermal optimum of several
443 eastern African lakes might be determined by local solar irradiance from Sep to Dec (maximum at ~6 cal ka BP) (Fig.
444 8) rather than northern hemisphere summer solar irradiance. The restratification processes of eastern African lakes in
445 these months and associated epilimnetic heating might explain the increased warming of lake water (Berke et al.,
446 2012a). However, modelling studies do not support this hypothesis (Dee et al., 2021).

447 In addition to local insolation changes, local changes in P/E could have the potential to modify the lake water temper-
448 ature. During the Early and Mid-Holocene, reconstructed high temperatures occurred during the African Humid Period,
449 accompanied by the wettest phase of Garba Guracha (Bittner et al., 2021) and rising lake levels in the region (Gasse,
450 2000; Junginger et al., 2014), indicating higher amounts of precipitation due to an intensification of the monsoon
451 system. A modelling study (Tierney et al., 2011b) proposes that during the AHP, the precipitation increase occurred
452 mainly in June, July, and August (JJA), shortening the duration of annual drought phases in eastern Africa. Increased
453 relative humidity would reduce evaporation, limiting the evaporative cooling of the lake water. Less evaporation, either
454 due to shorter drought phases or generally higher precipitation, would increase the temperature and cause less positive
455 $\delta^{18}\text{O}_{\text{lake water}}$ values, as suggested for Garba Guracha (Bittner et al., 2021).

456 The highest temperatures of the Holocene continued until 5.8 cal ka BP, interrupted only by a short drop in temperature
457 after 7 cal ka BP. This is in agreement with the Sacred Lake temperature record (Loomis et al., 2012). Lake Tana
458 experienced a shift towards colder conditions a bit earlier, from 7.5 to 7 cal ka BP (Loomis et al., 2015).

459 5.3.3. Cooling in the Late Holocene

460 After 5.8 cal ka BP, the MAT continuously decreased by ~3.6°C until recent times, coinciding with the summer inso-
461 lation decline and decreasing temperatures of equatorial lakes (Ivory and Russell, 2018), Lake Tana (Loomis et al.,
462 2015) and the marine Gulf of Aden record (Tierney et al., 2016). The general decreasing temperature trend is also
463 supported by $\delta^{18}\text{O}_{\text{lake water}}$, pollen and charcoal results showing a decrease in moisture availability and fire activity at
464 Garba Guracha (Bittner et al., 2021; Gil-Romera et al., 2019). Furthermore, an upwards shift of the lower and dry
465 forests during this time reinforces the idea of more intense evapotranspiration due to the decrease in moisture availa-
466 bility (Gil-Romera et al., 2021). A drop in TOC and decreasing $\delta^{13}\text{C}$ values (Bittner et al., 2020) support overall shifting
467 catchment conditions.

468 During the last two thousand years, we observed that the increasing temperature trend concurred with an abrupt in-
469 crease in the main woody communities and enhanced fire activities around Garba Guracha (Gil-Romera et al., 2021).
470 However, we cannot discard human influence favoring both woody encroachment and fire activity.

471 The strong connection of temperature, P/E and insolation across the Holocene shows that the Garba Guracha temper-
472 atures might have been affected by local radiation, possibly in interplay with insolation-driven atmospheric circulation
473 changes and their impacts on air mass source, cloud cover and evaporation. As current global warming continues, the
474 intense warming of landmasses could lead to a major and complex restructuring of the atmospheric circulation system
475 in the future, affecting eastern Africa and possibly even larger regions beyond via teleconnections.

476 **6. CONCLUSIONS**

477 Eastern African climatic history is spatially very diverse, and the driving mechanisms are complex and not fully un-
478 derstood. In eastern Africa, temperature reconstructions are generally sparse, especially in the high altitudes of the
479 Horn of Africa. In this study, we used brGDGT from a high-altitude sedimentary record of the Bale Mountains (lake
480 Garba Guracha, Southwestern Ethiopia) to produce the first temperature reconstruction for the Horn of Africa.

481 The composition of brGDGT isomers in sediment records is affected by several influences, mainly by MAT, but in
482 addition by lake water chemistry (pH and conductivity) and bacterial community, resulting in locally unique brGDGT
483 compositions. For instance, in some of the Bale Mountain lakes, the abundance of a specific isomer IIIa' is uncom-
484 monly high in surface sediments. However, the summed abundance of IIIa and IIIa' is similar to other comparable lake
485 archives in eastern Africa. We suspect that in the case of the Bale Mountains, changes in the lake's water chemistry
486 (pH and conductivity) or bacterial community are responsible for the high production of IIIa' at the expense of IIIa
487 under drier conditions. By including the 6 methyl isomer in a temperature calibration, we were able to enhance the
488 correlation with MAT. Therefore, we conclude that 6 methyl isomers have an impact on temperature reconstructions,
489 highlighting their inclusion in a Bale Mountain-specific temperature calibration. Using surface sediment data from
490 Bale Mountain lakes and the East African lake database, the best performing temperature calibration is a modified
491 MBT'_{SME} including IIIa'.

492 With the use of the new calibration, the Garba Guracha MAT record reflects insolation variability as one of the main
493 climatic drivers at millennial scales. Additional factors such as glacier and permafrost melting during deglaciation and

494 the regional atmospheric circulation likely play a prominent role on shorter time scales. These additional mechanisms
495 partly explain the asynchronicity between the Garba Guracha MAT record in the high altitude afro-alpine region of
496 the Horn of Africa and other eastern African lake records.

497 Further research is necessary to understand the influences on and the origin of brGDGTs producing communities,
498 especially at high altitudes.

499
500
501 **Author contribution.** LB, GGR, HFL, and MZ collected the samples. LB, CDJ, JMR and MZ developed the concept.
502 LB and CDJ extracted, analysed and interpreted the brGDGT data. LB led the manuscript writing with contributions
503 and feedback from all authors. MZ acquired the funding and supervised the work.

504 **Competing interests.** The authors declare that they have no conflict of interest.

505 **Acknowledgements**

506 This research was funded by the German Research Council (DFG: ZE 844/10–1) in the framework of the joint Ethio-
507 European DFG Research Unit 2358 "The Mountain Exile Hypothesis. How humans benefited from and reshaped
508 African high-altitude ecosystems during Quaternary climate changes". We are grateful to the project coordination, the
509 Philipps University Marburg, the University of Addis Abeba, the Frankfurt Zoological Society, the Ethiopian Wolf
510 Project, the Bale Mountains National Park, and the related staff members, especially Katinka Thielsen and Mekbib
511 Fekadu, for their logistic assistance during our fieldwork. We thank the Ethiopian Wildlife Conservation Authority for
512 permitting our research in the Bale Mountains National Park.

513

514 **7. REFERENCES**

515 Alley, R. B.: The Younger Dryas cold interval as viewed from central Greenland, *Quaternary Science Reviews*, 19,
516 213–226, [https://doi.org/https://doi.org/10.1016/S0277-3791\(99\)00062-1](https://doi.org/10.1016/S0277-3791(99)00062-1), 2000.

517 Baxter, A. J., Hopmans, E. C., Russell, J. M., and Sinninghe Damsté, J. S.: Bacterial GMGTs in East African lake
518 sediments: Their potential as palaeotemperature indicators, *Geochimica et Cosmochimica Acta*, 259, 155–169,
519 <https://doi.org/10.1016/j.gca.2019.05.039>, 2019.

520 Berke, M. A., Johnson, T. C., Werne, J. P., Schouten, S., and Sinninghe Damsté, J. S.: A mid-Holocene thermal

521 maximum at the end of the African Humid Period, *Earth and Planetary Science Letters*, 351–352, 95–104,
522 <https://doi.org/10.1016/j.epsl.2012.07.008>, 2012a.

523 Berke, M. A., Johnson, T. C., Werne, J. P., Grice, K., Schouten, S., and Sinninghe Damsté, J. S.: Molecular records of
524 climate variability and vegetation response since the Late Pleistocene in the Lake Victoria basin, East Africa,
525 *Quaternary Science Reviews*, 55, 59–74, <https://doi.org/10.1016/j.quascirev.2012.08.014>, 2012b.

526 Bini, M., Zanchetta, G., Perşoiu, A., Cartier, R., Català, A., Cacho, I., Dean, J. R., Di Rita, F., Drysdale, R. N., Finnè,
527 M., Isola, I., Jalali, B., Lirer, F., Magri, D., Masi, A., Marks, L., Mercuri, A. M., Peyron, O., Sadori, L., Sicre, M.-A.,
528 Welc, F., Zielhofer, C., and Brisset, E.: The 4.2 ka BP Event in the Mediterranean region: an overview, *Clim. Past*, 15,
529 555–577, <https://doi.org/10.5194/cp-15-555-2019>, 2019.

530 Bittner, L., Bliedtner, M., Grady, D., Gil-Romera, G., Martin-Jones, C., Lemma, B., Mekonnen, B., Lamb, H. F., Yang,
531 H., Glaser, B., Szidat, S., Salazar, G., Rose, N. L., Opgenoorth, L., Miehe, G., Zech, W., and Zech, M.: Revisiting
532 afro-alpine Lake Garba Guracha in the Bale Mountains of Ethiopia: rationale, chronology, geochemistry, and
533 paleoenvironmental implications, *Journal of Paleolimnology*, <https://doi.org/10.1007/s10933-020-00138-w>, 2020.

534 Bittner, L., Gil-Romera, G., Grady, D., Lamb, H. F., Lorenz, E., Weiner, M., Meyer, H., Bromm, T., Glaser, B., and
535 Zech, M.: The Holocene lake-evaporation history of the afro-alpine Lake Garba Guracha in the Bale Mountains,
536 Ethiopia, based on $\delta^{18}\text{O}$ records of sugar biomarker and diatoms, *Quaternary Research*, 1–14,
537 <https://doi.org/10.1017/qua.2021.26>, 2021.

538 Blom, R. G., Farr, T. G., Feynmann, J., Ruzmaikin, A., and Paillou, P.: The green Sahara: Climate change, hydrologic
539 history and human occupation, in: 2009 IEEE Radar Conference, 1–4, <https://doi.org/10.1109/RADAR.2009.4977129>,
540 2009.

541 Bonnefille, R., Chalié, F., Guiot, J., and Vincens, A.: Quantitative estimates of full glacial temperatures in equatorial
542 Africa from palynological data*, *Climate Dynamics*, 6, 251–257, <https://doi.org/10.1007/BF00193538>, 1992.

543 van Bree, L. G. J., Peterse, F., Baxter, A. J., De Crop, W., van Grinsven, S., Villanueva, L., Verschuren, D., and
544 Sinninghe Damsté, J. S.: Seasonal variability and sources of in situ brGDGT production in a permanently stratified
545 African crater lake, *Biogeosciences Discuss.*, 2020, 1–36, <https://doi.org/10.5194/bg-2020-233>, 2020.

546 Castañeda, I. S., Schouten, S., Pätzold, J., Lucassen, F., Kasemann, S., Kuhlmann, H., and Schefuß, E.: Hydroclimate
547 variability in the Nile River Basin during the past 28,000 years, *Earth and Planetary Science Letters*, 438, 47–56,
548 <https://doi.org/10.1016/j.epsl.2015.12.014>, 2016.

549 Cheddadi, R., Lamb, H. F., Guiot, J., and van der Kaars, S.: Holocene climatic change in Morocco: a quantitative

550 reconstruction from pollen data, *Climate Dynamics*, 14, 883–890, <https://doi.org/10.1007/s003820050262>, 1998.

551 Chevalier, M. and Chase, B. M.: Southeast African records reveal a coherent shift from high- to low-latitude forcing
552 mechanisms along the east African margin across last glacial–interglacial transition, *Quaternary Science Reviews*, 125,
553 117–130, <https://doi.org/10.1016/j.quascirev.2015.07.009>, 2015.

554 Costa, K., Russell, J., Konecky, B., and Lamb, H.: Isotopic reconstruction of the African Humid Period and Congo Air
555 Boundary migration at Lake Tana, Ethiopia, *Quaternary Science Reviews*, 83, 58–67,
556 <https://doi.org/10.1016/j.quascirev.2013.10.031>, 2014.

557 Damsté, J. S. S., Hopmans, E. C., Pancost, R. D., Schouten, S., and Geenevasen, J. A. J.: Newly discovered non-
558 isoprenoid glycerol dialkyl glycerol tetraether lipids in sediments, *Chemical Communications*, 1683–1684,
559 <https://doi.org/10.1039/b004517i>, 2000.

560 Dearing Crampton-Flood, E., Tierney, J. E., Peterse, F., Kirkels, F. M. S. A., and Sinninghe Damsté, J. S.: BayMBT:
561 A Bayesian calibration model for branched glycerol dialkyl glycerol tetraethers in soils and peats, *Geochimica et*
562 *Cosmochimica Acta*, 268, 142–159, <https://doi.org/https://doi.org/10.1016/j.gca.2019.09.043>, 2020.

563 Dee, S. G., Morrill, C., Kim, S. H., and Russell, J. M.: Hot Air, Hot Lakes, or Both? Exploring Mid-Holocene African
564 Temperatures Using Proxy System Modeling, *Journal of Geophysical Research: Atmospheres*, 126, e2020JD033269,
565 <https://doi.org/https://doi.org/10.1029/2020JD033269>, 2021.

566 deMenocal, P., Ortiz, J., Guilderson, T., Adkins, J., Sarnthein, M., Baker, L., and Yarusinsky, M.: Abrupt onset and
567 termination of the African Humid Period:, *Quaternary Science Reviews*, 19, 347–361, [https://doi.org/10.1016/S0277-](https://doi.org/10.1016/S0277-3791(99)00081-5)
568 [3791\(99\)00081-5](https://doi.org/10.1016/S0277-3791(99)00081-5), 2000.

569 Eggermont, Windafraash, M., Van Damme, M., Lens, K., and Umer M., H.: Bale Moluntains Lakes : Ecosystems under
570 pressure of global change?, *Walia*, 2011, 171–180, https://doi.org/10.10520/AJA00837059_148, 2011.

571 Eggermont, H., Heiri, O., James, A., Ae, R., Vuille, M., Leen, A., Ae, A., and Verschuren, D.: Paleotemperature
572 reconstruction in tropical Africa using fossil Chironomidae (Insecta: Diptera), *Journal of Paleolimnology*, 43, 413–
573 435, <https://doi.org/10.1007/s10933-009-9339-2>, 2010.

574 Garelick, S., Russell, J., Richards, A., Smith, J., Kelly, M., Anderson, N., Jackson, M. S., Doughty, A., Nakileza, B.,
575 Ivory, S., Dee, S., and Marshall, C.: The dynamics of warming during the last deglaciation in high-elevation regions
576 of Eastern Equatorial Africa, *Quaternary Science Reviews*, 281, 107416,
577 <https://doi.org/10.1016/j.quascirev.2022.107416>, 2022.

578 Gasse, F.: Hydrological changes in the African tropics since the Last Glacial Maximum, *Quaternary Science Reviews*,

579 19, 189–211, [https://doi.org/https://doi.org/10.1016/S0277-3791\(99\)00061-X](https://doi.org/https://doi.org/10.1016/S0277-3791(99)00061-X), 2000.

580 Gil-Romera, G., Adolf, C., Benito Blas, M., Bittner, L., Johansson, M. M. U., Grady, D. D. A., Lamb, H. H. F., Lemma,
581 B., Fekadu, M., Glaser, B., Mekonnen, B., Sevilla-Callejo, M., Zech, M., Zech, W., Mieke, G., Benito, B. M., Bittner,
582 L., Johansson, M. M. U., Grady, D. D. A., Lamb, H. H. F., Lemma, B., Fekadu, M., Glaser, B., Mekonnen, B., Sevilla-
583 Callejo, M., Zech, M., Zech, W., and Mieke, G.: Long-term fire resilience of the Ericaceous Belt, Bale Mountains,
584 Ethiopia, *Biology Letters*, 15, 20190357, <https://doi.org/10.1098/rsbl.2019.0357>, 2019.

585 Gil-Romera, G., Fekadu, M., Opgenoorth, L., Grady, D., Lamb, H. F., Bittner, L., Zech, M., and Mieke, G.: The new
586 Garba Guracha palynological sequence: Revision and data expansion, in: *Quaternary Vegetation Dynamics – The*
587 *African Pollen Database*, edited by: Runge, J., Gosling, W.D., Lézine, A-M., S. L., CRC Press, London, 442,
588 <https://doi.org/10.1201/9781003162766>, 2021.

589 Groos, A., Akçar, N., Yesilyurt, S., Mieke, G., Vockenhuber, C., and Veit, H.: Nonuniform Late Pleistocene glacier
590 fluctuations in tropical Eastern Africa, *Science Advances*, 7, <https://doi.org/10.1126/sciadv.abb6826>, 2021.

591 Groos, A. R., Niederhauser, J., Wraase, L., Hänsel, F., Nauss, T., Akçar, N., and Veit, H.: Implications of present
592 ground temperatures and relict stone stripes in the Ethiopian Highlands for the palaeoclimate of the tropics, *Earth Surf.*
593 *Dynam. Discuss.*, 2020, 1–37, <https://doi.org/10.5194/esurf-2020-53>, 2020.

594 Hillman, J.: *The Bale Mountains National Park Area, Southeast Ethiopia, and Its Management*, 253 pp.,
595 <https://doi.org/10.2307/3673456>, 1988.

596 Hopmans, E. C., Weijers, J. W. H., Schefuß, E., Herfort, L., Sinninghe Damsté, J. S., and Schouten, S.: A novel proxy
597 for terrestrial organic matter in sediments based on branched and isoprenoid tetraether lipids, *Earth and Planetary*
598 *Science Letters*, 224, 107–116, <https://doi.org/10.1016/j.epsl.2004.05.012>, 2004.

599 Hopmans, E. C., Schouten, S., and Sinninghe Damsté, J. S.: The effect of improved chromatography on GDGT-based
600 palaeoproxies, *Organic Geochemistry*, 93, 1–6, <https://doi.org/https://doi.org/10.1016/j.orggeochem.2015.12.006>,
601 2016.

602 Hove, H., Echeverria, D., and Parry, J.-E.: *Review of current and planned adaptation action: East Africa*, International
603 Institute for Sustainable Development, Winnipeg, 2011.

604 Hughes, A. C., Orr, M. C., Ma, K., Costello, M. J., Waller, J., Provoost, P., Yang, Q., Zhu, C., and Qiao, H.: Sampling
605 biases shape our view of the natural world, *Ecography*, 44, 1259–1269,
606 <https://doi.org/https://doi.org/10.1111/ecog.05926>, 2021.

607 Huguet, C., Kim, J. H., Damsté, J. S. S., and Schouten, S.: Reconstruction of sea surface temperature variations in the

608 Arabian Sea over the last 23 kyr using organic proxies (TEX86 and U₃₇K'), *Paleoceanography*, 21,
609 <https://doi.org/10.1029/2005PA001215>, 2006.

610 Huybers, P.: Early Pleistocene Glacial Cycles and the Integrated Summer Insolation Forcing, *Science* (New York,
611 N.Y.), 313, 508–511, <https://doi.org/10.1126/science.1125249>, 2006.

612 IPCC: Climate Change 2021: The Physical Science Basis. Contribution of Working Group I to the Sixth Assessment
613 Report of the Intergovernmental Panel on Climate Change [Masson-Delmotte, V., P. Zhai, A. Pirani, S.L. Connors, C.
614 Péan, S. Berger, N. Caud, Y. Chen, Cambridge University Press, 2021.

615 Ivory, S. J. and Russell, J.: Lowland forest collapse and early human impacts at the end of the African Humid Period
616 at Lake Edward, equatorial East Africa, *Quaternary Research*, 89, 7–20, <https://doi.org/10.1017/qua.2017.48>, 2018.

617 Jaeschke, A., Thienemann, M., Schefuß, E., Urban, J., Schäbitz, F., Wagner, B., and Rethemeyer, J.: Holocene
618 Hydroclimate Variability and Vegetation Response in the Ethiopian Highlands (Lake Dendi), *Frontiers in Earth
619 Science*, 8, 1–14, <https://doi.org/10.3389/feart.2020.585770>, 2020.

620 De Jonge, C., Hopmans, E. C., Zell, C. I., Kim, J.-H., Schouten, S., and Sinninghe Damsté, J. S.: Occurrence and
621 abundance of 6-methyl branched glycerol dialkyl glycerol tetraethers in soils: Implications for palaeoclimate
622 reconstruction, *Geochimica et Cosmochimica Acta*, 141, 97–112, <https://doi.org/10.1016/j.gca.2014.06.013>, 2014.

623 De Jonge, C., Radujković, D., Sigurdsson, B. D., Weedon, J. T., Janssens, I., and Peterse, F.: Lipid biomarker
624 temperature proxy responds to abrupt shift in the bacterial community composition in geothermally heated soils,
625 *Organic Geochemistry*, 137, <https://doi.org/10.1016/j.orggeochem.2019.07.006>, 2019.

626 De Jonge, C., Kuramae, E. E., Radujković, D., Weedon, J. T., Janssens, I. A., and Peterse, F.: The influence of soil
627 chemistry on branched tetraether lipids in mid- and high latitude soils: Implications for brGDGT- based
628 paleothermometry, *Geochimica et Cosmochimica Acta*, 310, 95–112,
629 <https://doi.org/https://doi.org/10.1016/j.gca.2021.06.037>, 2021.

630 Junginger, A., Roller, S., Olaka, L. A., and Trauth, M. H.: The effects of solar irradiation changes on the migration of
631 the Congo Air Boundary and water levels of paleo-Lake Suguta , Northern Kenya Rift , during the African Humid
632 Period (15 – 5 ka BP), *Palaeogeography, Palaeoclimatology, Palaeoecology*, 396, 1–16,
633 <https://doi.org/10.1016/j.palaeo.2013.12.007>, 2014.

634 Kassambara, A. and Mundt, F.: factoextra: Extract and Visualise the Results of Multivariate Data Analyses,
635 <https://cran.r-project.org/package=factoextra>, 2020.

636 Kidane, Y., Stahlmann, R., and Beierkuhnlein, C.: Vegetation dynamics, and land use and land cover change in the

637 Bale Mountains, Ethiopia, *Environmental Monitoring and Assessment*, 184, 7473–7489,
638 <https://doi.org/10.1007/s10661-011-2514-8>, 2012.

639 Laskar, J., Robutel, P., Joutel, F., Gastineau, M., Correia, A. C. M., and Levrard, B.: A long-term numerical solution
640 for the insolation quantities of the Earth, *A&A*, 428, 261–285, 2004.

641 Löffler, H.: Limnology and paleolimnological data on the Bale Mountain Lakes, Verth, International Verein.
642 *Limnology*, 20, 1131–1138, 1978.

643 Loomis, S. E., Russell, J. M., and Sinninghe Damsté, J. S.: Distributions of branched GDGTs in soils and lake
644 sediments from western Uganda: Implications for a lacustrine paleothermometer, *Organic Geochemistry*, 42, 739–751,
645 <https://doi.org/10.1016/j.orggeochem.2011.06.004>, 2011.

646 Loomis, S. E., Russell, J. M., Heures, A. M., D'Andrea, W. J., and Sinninghe Damsté, J. S.: Seasonal variability of
647 branched glycerol dialkyl glycerol tetraethers (brGDGTs) in a temperate lake system, *Geochimica et Cosmochimica*
648 *Acta*, 144, 173–187, <https://doi.org/10.1016/j.gca.2014.08.027>, 2014.

649 Loomis, S. E., Russell, J. M., and Lamb, H. F.: Northeast African temperature variability since the Late Pleistocene,
650 *Palaeogeography, Palaeoclimatology, Palaeoecology*, 423, 80–90, <https://doi.org/10.1016/j.palaeo.2015.02.005>, 2015.

651 Loomis, S. E., Russell, J. M., Verschuren, D., Morrill, C., De Cort, G., Sinninghe Damsté, J. S., Olago, D., Eggermont,
652 H., Street-Perrott, F. A., and Kelly, M. A.: The tropical lapse rate steepened during the Last Glacial Maximum, *Science*
653 *Advances*, 3, <https://doi.org/10.1126/sciadv.1600815>, 2017.

654 Loomis, S. E. S. E., Russell, J. M., Ladd, B., Street-Perrott, F. A. A., and Sinninghe Damsté, J. S. J. S.: Calibration
655 and application of the branched GDGT temperature proxy on East African lake sediments, *Earth and Planetary Science*
656 *Letters*, 357–358, 277–288, <https://doi.org/https://doi.org/10.1016/j.epsl.2012.09.031>, 2012.

657 Lyon, B. and Vigaud, N.: Unraveling East Africa's Climate Paradox,
658 <https://doi.org/https://doi.org/10.1002/9781119068020.ch16>, 22 June 2017.

659 Marshall, M., Lamb, H., Davies, S., Leng, M., Bedaso, Z., Umer, M., and Bryant, C.: Climatic change in northern
660 Ethiopia during the past 17,000 years: A diatom and stable isotope record from Lake Ashenge, *Palaeogeography*
661 *Palaeoclimatology Palaeoecology*, 279, <https://doi.org/10.1016/j.palaeo.2009.05.003>, 2009.

662 Martínez-Sosa, P., Tierney, J. E., Stefanescu, I. C., Crampton-Flood, E. D., Shuman, B. N., and Routson, C.: A global
663 Bayesian temperature calibration for lacustrine brGDGTs, <https://doi.org/10.1594/PANGAEA.931169>, 6 May 2021.

664 Miehe, S. and Miehe, G.: Ericaceous forests and heathlands in the Bale mountains of South Ethiopia : ecology and
665 man's impact, edited by: Miehe, G. and 1952-, Reinbek : Warnke, Reinbek, 1994.

666 Morrissey, A. and Scholz, C. A. C. A. C. A.: Paleohydrology of Lake Turkana and its influence on the Nile River
667 system, *Palaeogeography, Palaeoclimatology, Palaeoecology*, 403, 88–100,
668 <https://doi.org/https://doi.org/10.1016/j.palaeo.2014.03.029>, 2014.

669 Morrissey, A., Scholz, C. A., and Russell, J. M.: Late Quaternary TEX₈₆ paleotemperatures from the world's largest
670 desert lake, Lake Turkana, Kenya, *Journal of Paleolimnology*, 59, 103–117, [https://doi.org/10.1007/s10933-016-9939-](https://doi.org/10.1007/s10933-016-9939-6)
671 6, 2018.

672 Neukom, R., Barboza, L. A., Erb, M. P., Shi, F., Emile-Geay, J., Evans, M. N., Franke, J., Kaufman, D. S., Lücke, L.,
673 Rehfeld, K., Schurer, A., Zhu, F., Brönnimann, S., Hakim, G. J., Henley, B. J., Ljungqvist, F. C., McKay, N., Valler,
674 V., von Gunten, L., and Consortium, P. 2k: Consistent multidecadal variability in global temperature reconstructions
675 and simulations over the Common Era, *Nature Geoscience*, 12, 643–649, <https://doi.org/10.1038/s41561-019-0400-0>,
676 2019.

677 Nicholson, S. E.: Climate and climatic variability of rainfall over eastern Africa, *Reviews of Geophysics*, 55, 590–635,
678 <https://doi.org/https://doi.org/10.1002/2016RG000544>, 2017.

679 Osmaston, H. A., Mitchell, W. A., and Osmaston, J. A. N.: Quaternary glaciation of the Bale Mountains, Ethiopia,
680 *Journal of Quaternary Science*, 20, 593–606, <https://doi.org/10.1002/jqs.931>, 2005.

681 Ossendorf, G., Groos, A., Bromm, T., Girma Tekelemariam, M., Glaser, B., Lesur, J., Schmidt, J., Akçar, N., Bekele,
682 T., Beldados, A., Demissew, S., Hadush Kahsay, T., P Nash, B., Nauss, T., Negash, A., Nemomissa, S., Veit, H.,
683 Vogelsang, R., Zerihun, W., and Mieke, G.: Middle Stone Age foragers resided in high elevations of the glaciated Bale
684 Mountains, Ethiopia, *Science*, 365, 583–587, 2019.

685 Otto-Bliesner, B. L., Russell, J. M., Clark, P. U., Liu, Z., Overpeck, J. T., Konecky, B., DeMenocal, P., Nicholson, S.
686 E., He, F., and Lu, Z.: Coherent changes of south-eastern equatorial and northern African rainfall during the last
687 deglaciation, *Science*, 346, 1223–1227, <https://doi.org/10.1126/science.1259531>, 2014.

688 Peterse, F., van der Meer, J., Schouten, S., Weijers, J. W. H., Fierer, N., Jackson, R. B., Kim, J.-H., and Sinninghe
689 Damsté, J. S.: Revised calibration of the MBT–CBT paleotemperature proxy based on branched tetraether membrane
690 lipids in surface soils, *Geochimica et Cosmochimica Acta*, 96, 215–229,
691 <https://doi.org/https://doi.org/10.1016/j.gca.2012.08.011>, 2012.

692 Powers, L. A., Johnson, T. C., Werne, J. P., Castañeda, I. S., Hopmans, E. C., Sinninghe Damsté, J. S., and Schouten,
693 S.: Large temperature variability in the southern African tropics since the Last Glacial Maximum, *Geophysical*
694 *Research Letters*, 32, 1–4, <https://doi.org/10.1029/2004GL022014>, 2005.

695 R Core Team: R: A Language and Environment for Statistical Computing, <https://www.r-project.org/>, 2021.

696 Raberg, J. H., Harning, D. J., Crump, S. E., de Wet, G., Blumm, A., Kopf, S., Geirsdóttir, Á., Miller, G. H., and
697 Sepúlveda, J.: Revised fractional abundances and warm-season temperatures substantially improve brGDGT
698 calibrations in lake sediments, *Biogeosciences*, 18, 3579–3603, <https://doi.org/10.5194/bg-18-3579-2021>, 2021.

699 Russell, J. M., Hopmans, E. C., Loomis, S. E., Liang, J., and Sinninghe Damsté, J. S.: Distributions of 5- and 6-methyl
700 branched glycerol dialkyl glycerol tetraethers (brGDGTs) in East African lake sediment: Effects of temperature, pH,
701 and new lacustrine paleotemperature calibrations, *Organic Geochemistry*, 117, 56–69,
702 <https://doi.org/10.1016/j.orggeochem.2017.12.003>, 2018.

703 Schouten, S., Forster, A., Panoto, F. E., and Sinninghe Damsté, J. S.: Towards calibration of the TEX₈₆
704 palaeothermometer for tropical sea surface temperatures in ancient greenhouse worlds, *Organic Geochemistry*, 38,
705 1537–1546, <https://doi.org/10.1016/j.orggeochem.2007.05.014>, 2007.

706 Schreuder, L. T., Beets, C. J., Prins, M. A., Hatté, C., and Peterse, F.: Late Pleistocene climate evolution in Southeastern
707 Europe recorded by soil bacterial membrane lipids in Serbian loess, *Palaeogeography, Palaeoclimatology,*
708 *Palaeoecology*, 449, 141–148, <https://doi.org/10.1016/j.palaeo.2016.02.013>, 2016.

709 Sinninghe Damsté, J. S., Rijpstra, W. I. C., Foesel, B. U., Huber, K. J., Overmann, J., Nakagawa, S., Kim, J. J.,
710 Dunfield, P. F., Dedysh, S. N., and Villanueva, L.: An overview of the occurrence of ether- and ester-linked iso-
711 diabolic acid membrane lipids in microbial cultures of the Acidobacteria: Implications for brGDGT paleoproxies for
712 temperature and pH, *Organic Geochemistry*, 124, 63–76, <https://doi.org/10.1016/j.orggeochem.2018.07.006>, 2018.

713 Tiercelin, J. J., Gibert, E., Umer, M., Bonnefille, R., Disnar, J. R., Lézine, A. M., Hureau-Mazaudier, D., Travi, Y.,
714 Keravis, D., and Lamb, H. F.: High-resolution sedimentary record of the last deglaciation from a high-altitude lake in
715 Ethiopia, *Quaternary Science Reviews*, 27, 449–467, <https://doi.org/10.1016/j.quascirev.2007.11.002>, 2008.

716 Tierney, J. E. and deMenocal, P. B.: Abrupt Shifts in Horn of Africa Hydroclimate Since the Last Glacial Maximum,
717 *Science*, 342, 843–846, <https://doi.org/10.1126/science.1240411>, 2013.

718 Tierney, J. E. and Russell, J. M.: Abrupt climate change in southeast tropical Africa influenced by Indian monsoon
719 variability and ITCZ migration, *Geophysical Research Letters*, 34, <https://doi.org/10.1029/2007GL029508>, 2007.

720 Tierney, J. E., Russell, J. M., Huang, Y., Damste, J. S. S., Hopmans, E. C., and Cohen, A. S.: Northern Hemisphere
721 Controls on Tropical Southeast African Climate During the Past 60,000 Years, *Science*, 322, 252–255,
722 <https://doi.org/10.1126/science.1160485>, 2008.

723 Tierney, J. E., Russell, J. M., Sinninghe Damsté, J. S., Huang, Y., and Verschuren, D.: Late Quaternary behavior of

724 the East African monsoon and the importance of the Congo Air Boundary, *Quaternary Science Reviews*, 30, 798–807,
725 <https://doi.org/10.1016/j.quascirev.2011.01.017>, 2011a.

726 Tierney, J. E., Lewis, S. C., Cook, B. I., LeGrande, A. N., and Schmidt, G. A.: Model, proxy and isotopic perspectives
727 on the East African Humid Period, *Earth and Planetary Science Letters*, 307, 103–112,
728 <https://doi.org/10.1016/j.epsl.2011.04.038>, 2011b.

729 Tierney, J. E., Smerdon, J. E., Anchukaitis, K. J., and Seager, R.: Multidecadal variability in East African hydroclimate
730 controlled by the Indian Ocean, *Nature*, 493, 389–392, <https://doi.org/10.1038/nature11785>, 2013.

731 Tierney, J. E., Pausata, F. S. R., and Demenocal, P.: Deglacial Indian monsoon failure and North Atlantic stadials
732 linked by Indian Ocean surface cooling, *Nature Geoscience*, 9, 46–50, <https://doi.org/10.1038/ngeo2603>, 2016.

733 Tierney, J. E., Pausata, F. S. R., and DeMenocal, P. B.: Rainfall regimes of the Green Sahara, *Science Advances*, 3,
734 <https://doi.org/10.1126/sciadv.1601503>, 2017.

735 Trauth, M. H., Foerster, V., Junginger, A., Asrat, A., Lamb, H. F., and Schaebitz, F.: Abrupt or gradual? Change point
736 analysis of the late Pleistocene–Holocene climate record from Chew Bahir, southern Ethiopia, *Quaternary Research*,
737 90, 321–330, [https://doi.org/DOI: 10.1017/qua.2018.30](https://doi.org/DOI:10.1017/qua.2018.30), 2018.

738 Uhlig, S. and Uhlig, K.: Studies on the Altitudinal Zonation of Forests and Alpine Plants in the Central Bale Mountains,
739 Ethiopia, 153 pp., <https://doi.org/10.2307/3673574>, 1991.

740 Uhlig, S. K.: Mountain Forests and the Upper Tree Limit on the Southeastern Plateau of Ethiopia, *Mountain Research*
741 *and Development*, 8, 227–234, <https://doi.org/10.2307/3673452>, 1988.

742 Umer, M., Lamb, H. F., Bonnefille, R., Lézine, A. M., Tiercelin, J. J., Gibert, E., Cazet, J. P., and Watrin, J.: Late
743 Pleistocene and Holocene vegetation history of the Bale Mountains, Ethiopia, *Quaternary Science Reviews*, 26, 2229–
744 2246, <https://doi.org/10.1016/j.quascirev.2007.05.004>, 2007.

745 Wagner, B., Wennrich, V., Viehberg, F., Junginger, A., Kolvenbach, A., Rethemeyer, J., Schaebitz, F., and Schmiedl,
746 G.: Holocene rainfall runoff in the central Ethiopian highlands and evolution of the River Nile drainage system as
747 revealed from a sediment record from Lake Dendi, *Global and Planetary Change*, 163, 29–43,
748 <https://doi.org/10.1016/j.gloplacha.2018.02.003>, 2018.

749 Wang, H., Liu, W., He, Y., Zhou, A., Zhao, H., Liu, H., Cao, Y., Hu, J., Meng, B., Jiang, J., Kolpakova, M.,
750 Krivonogov, S., and Liu, Z.: Salinity-controlled isomerisation of lacustrine brGDGTs impacts the associated
751 MBT5ME' terrestrial temperature index, *Geochimica et Cosmochimica Acta*, 305, 33–48,
752 <https://doi.org/https://doi.org/10.1016/j.gca.2021.05.004>, 2021.

753 Weber, Y., Damsté, J. S. S., Zopfi, J., De Jonge, C., Gilli, A., Schubert, C. J., Lepori, F., Lehmann, M. F., and Niemann,
754 H.: Redox-dependent niche differentiation provides evidence for multiple bacterial sources of glycerol tetraether lipids
755 in lakes, *Proceedings of the National Academy of Sciences of the United States of America*, 115, 10926–10931,
756 <https://doi.org/10.1073/pnas.1805186115>, 2018.

757 Weijers, J. W. H., Schefuß, E., Schouten, S., and Damsté, J. S. S.: Coupled thermal and hydrological evolution of
758 tropical Africa over the last deglaciation, *Science*, 315, 1701–1704, <https://doi.org/10.1126/science.1138131>, 2007a.

759 Weijers, J. W. H., Schouten, S., van den Donker, J. C., Hopmans, E. C., and Sinninghe Damsté, J. S.: Environmental
760 controls on bacterial tetraether membrane lipid distribution in soils, *Geochimica et Cosmochimica Acta*, 71, 703–713,
761 <https://doi.org/10.1016/j.gca.2006.10.003>, 2007b.

762 Werdecker, J.: Eine Durchquerung des Goba-Massivs in Südäthiopien, *Hermann vo*, 132–144, 1962.

763 Williams, F. M.: *The Southeastern Highlands and the Ogaden*, edited by: Williams, F. M., Springer International
764 Publishing, Cham, 153–170, https://doi.org/10.1007/978-3-319-02180-5_15, 2016.

765 Woldu, Z., Feoli, E., and Nigatu, L.: Partitioning an elevation gradient of vegetation from south-eastern Ethiopia by
766 probabilistic methods, *Plant Ecology*, 81, 189–198, 1989.

767 Wu, H., Guiot, J., Brewer, S., and Guo, Z.: Climatic changes in Eurasia and Africa at the last glacial maximum and
768 mid-Holocene: reconstruction from pollen data using inverse vegetation modelling, *Climate Dynamics*, 29, 211–229,
769 <https://doi.org/10.1007/s00382-007-0231-3>, 2007.

770 Zeng, F. and Yang, H.: Temperature changes reconstructed from branched GDGTs on the central Loess Plateau during
771 the past 130–5 ka, *Quaternary International*, 503, 3–9, <https://doi.org/https://doi.org/10.1016/j.quaint.2018.04.045>,
772 2019.

773